Geothermal Energy

RESEARCH

Open Access

Hydrogeochemical and microbial characterization of a Middle Triassic carbonate aquifer (Muschelkalk) in Berlin and geochemical simulation of its use as a high-temperature aquifer thermal energy storage

Lioba Virchow[1*], Christian Siever-Wenzlaff[2], Guido Blöcher[1], Armando Alibrandi[1], Jens Kallmeyer[1], Martin Zimmer[1], Thomas Wiersberg[1], Christoph Thielke[3], Anja Schleicher[1] and Simona Regenspurg[1]

*Correspondence:
lioba.virchow@gfz-potsdam.de

[1] Helmholtz Centre Potsdam, GFZ German Research Centre for Geoscience, Telegrafenberg, 14473 Potsdam, Germany
[2] GASAG Solution Plus GmbH, EUREF-Campus 23-24, 10829 Berlin, Germany
[3] BEW Berliner Energie und Wärme AG, Hildegard-Knef-Platz 2, 10829 Berlin, Germany

Abstract

The geological formation of the Muschelkalk is widespread in the center of the North German Basin (NGB) and is increasingly attracting interest for application of geothermal energy extraction or high-temperature aquifer thermal energy storage (HT-ATES). This study investigates the Middle Triassic *"Rüdersdorfer Schaumkalk"*, which was the former injection horizon of the natural gas storage facility in Berlin, Germany. For the first time, detailed chemical and microbiological analyses of formation water of this Lower Muschelkalk limestone formation were conducted and hydrogeochemically characterized. In addition, a hydrogeochemical model was developed to quantify the potential reactions during HT-ATES focusing on calcite dissolution and precipitation. The main objectives of this study are: (1) to determine the origin of the water from the three wells targeting the Muschelkalk aquifer, (2) to understand changes in hydrochemistry after system operation, and (3) to evaluate the long-term sustainability of a potential HT-ATES system with increasing temperature. The target formation is encountered by several wells at about 525 m below the surface with an average thickness of 30 m. Two hydraulic lifting tests including physical, chemical, and microbial groundwater as well as gas monitoring were carried out. In addition, several downhole samples of formation fluid were collected from the aquifer at in situ pressure and temperature conditions. Fluid analysis of the saline formation water indicate a seawater origin within the Muschelkalk with subsequent evaporation and various water–rock interactions with anhydrite/gypsum, dolomite, and calcite. With a salinity of 130 g/L, dominated by Na–Cl, a slightly acidic pH between 6 and 7, and a low gas content of 3%, the formation water fits to other saline deep formation waters of the NGB. Gas concentrations and microbial communities like sulfate-reducing bacteria and methanogenic archaea in the produced water indicate several geochemical alterations and microbial processes like corrosion and the forming of biogenic methane. Geochemical simulations of calcite equilibrium over 10 HT-ATES cycles indicated a pronounced propensity for calcite precipitation up to 31 mg/kgw, within the heat exchanger. At the same

© The Author(s) 2024. **Open Access** This article is licensed under a Creative Commons Attribution 4.0 International License, which permits use, sharing, adaptation, distribution and reproduction in any medium or format, as long as you give appropriate credit to the original author(s) and the source, provide a link to the Creative Commons licence, and indicate if changes were made. The images or other third party material in this article are included in the article's Creative Commons licence, unless indicated otherwise in a credit line to the material. If material is not included in the article's Creative Commons licence and your intended use is not permitted by statutory regulation or exceeds the permitted use, you will need to obtain permission directly from the copyright holder. To view a copy of this licence, visit http://creativecommons.org/licenses/by/4.0/.

time, these models predicted a significant potential for calcite dissolution, with rates up to 21 mg/kgw, in both the cold and hot reservoirs. The results from the carbonate aquifer characterized in this study can be transferred to other sites in the NGB affected by salt tectonics and have provided information on the microbiological-chemical processes to be expected during the initial use of old wells.

Keywords: HT-ATES, Carbonate aquifer, Calcite precipitation, Geochemical modeling, North German Basin, Muschelkalk

Introduction

The use of fossil fuels, particularly oil and gas, has a long history in Germany and has played a significant role in the country's energy supply. Over time, numerous gas and oil wells have been drilled to exploit and extract these resources or store gas underground. With a growing awareness of the need for decarbonization and the reduction of greenhouse gas emissions, questions arise about the future use of these former wells. As part of the transition to a low-carbon energy supply, alternative uses for this drilling infrastructure are being explored to contribute to the heat transition and achieve climate goals.

One promising technology that can be innovatively utilized from existing drilling infrastructure is HT-ATES. The term HT-ATES is generally used for injection temperatures above 40 °C (Fleuchaus et al. 2018), whereby the aquifers usually extend to medium depth. While the share of renewables in the electricity sector is steadily increasing, it is stagnating in the heat sector, despite the fact that in Berlin, for example, almost half of CO_2 emissions are caused by the heating sector (Hirschl et al. 2021). HT-ATES can be a possibility to master the challenges of the acyclic heat demand and supply by storing the surplus heat in an aquifer and discharging it during periods of heat demand. ATES, thus, represents a cost-efficient storage technology that reduces energy consumption and CO_2 emissions (Daniilidis et al. 2022). Due to the ability to store large volumes in the underground while at the same time requiring little space on the surface, ATES systems are particularly suitable for urban areas.

The application of HT-ATES appears particularly promising in the city of Berlin, Germany, where former gas wells, such as the old gas storage facility in Berlin Spandau, which was decommissioned in 2017, offer optimal conditions to investigate the use of HT-ATES in carbonate rock and explore the possibility of repurposing old wells. While most ATES research sites have been limited to siliciclastic aquifers thus far (Fleuchaus et al. 2018), this approach opens up new opportunities for the utilization of HT-ATES in carbonate aquifers. Simultaneously, this provides the unique and first-ever opportunity to characterize a Muschelkalk aquifer in the North German Basin.

Although ATES was developed in the 1960s, it fell out of focus for a period due to geochemical processes that clogged plant parts and aquifers (Fleuchaus et al. 2018). However, in the past decade, HT-ATES has regained increased attention in research. Since 2021, a large-scale HT-ATES demonstration project is running in Middenmeer, the Netherlands (Oerlemans et al. 2022). And yet, even though the need for storage technologies is growing and an increasing amount of research is being done, e.g., Beernink et al. (2024); Blöcher et al. (2024); Collignon et al. (2020); Fleuchaus et al. (2018); Holmslykke

et al. (2023); Stricker et al. (2024), the aquifer storage of the parliament buildings in Berlin is the only functioning HT-ATES, although it has hardly been in operation since 2007 (Fleuchaus et al. 2021).

Injecting hot water into a colder aquifer may negatively impact its performance due to shifting the natural biogeochemical equilibrium. This could cause mineral precipitation or dissolution and corrosion processes (Brons et al. 1991; Griffioen and Appelo 1993; Holm et al. 1987; Jenne 1992), thus changing the hydraulic permeability in the aquifer (Holmslykke and Kjøller, 2023; Holmslykke et al. 2023), clogging of the plant, or aging of the plant components, which significantly affects the ATES's efficiency and lifespan. Temperature increases can change the thermodynamic equilibrium, reaction kinetics, microbial abundance, redox states, pH, sorption reactions, and cause mobilization of substances. Specifically, there is a high risk of carbonate precipitation, because calcite exhibits retrograde solubility, i.e., saturation increases with increasing temperature. In addition, the saturation of carbonates is a function of the increase and decrease in pressure and the associated degassing, with pCO_2 impacting the pH. The aforementioned processes require a comprehensive initial characterization of potential ATES reservoirs, examining inorganic, organic, gas, solid phases, and microbial activity to predict and manage these reactions.

The main objectives of this study are: (1) to determine the origin of the water from the three wells used as gas storage site targeting the Muschelkalk aquifer, (2) to characterize the formation water and the geochemical and microbial processes in the wellbores, and (3) to simulate changes in hydrochemistry before and after system operation and evaluate the long-term sustainability of a potential HT-ATES system with increasing temperature.

Materials and methods

Geological setting and former usage of the study area

The study area is the former Berlin natural gas storage facility in Spandau, Berlin, Germany. It is located within the central region of the Germanic Basin. After the formation of the Central European Basin during the Permian period, cyclic transgressions and regressions led to the deposition of Zechstein evaporites. Subsequently, with the closure of the portals to the Tethys during the Lower Triassic Bunter, continental sediments accumulated in the basin. The resurgence of marine ingressions occurred during the Muschelkalk period, resulting in the deposition of shallow marine carbonates beneath the wave base in the Muschelkalk Sea (Jubitz 1994). In shallow regions, such as present-day Berlin and Brandenburg, the deposition of the Lower Muschelkalk Schaumkalk formation occurred, which interfingered with the Jena Formation along its edges (Franz et al. 2020) (Fig. 1). Following the evaporite formation due to the depression's closure in the Middle Muschelkalk, the Upper Muschelkalk period marked the basin's reconnection with the ocean, leading to the accumulation of marine carbonates (Hagdorn et al. 2019). Afterward, during the Keuper period, the environment returned to continental conditions, resulting in the deposition of marl and sandstone layers.

The Muschelkalk in the NGB has an average thickness of 200 to 300 m and is mostly exposed at depths of several thousand meters (Franz et al. 2020). An exception is the Rüdersdorf outcrop, located 40 km to the east, where the Rüdersdorf

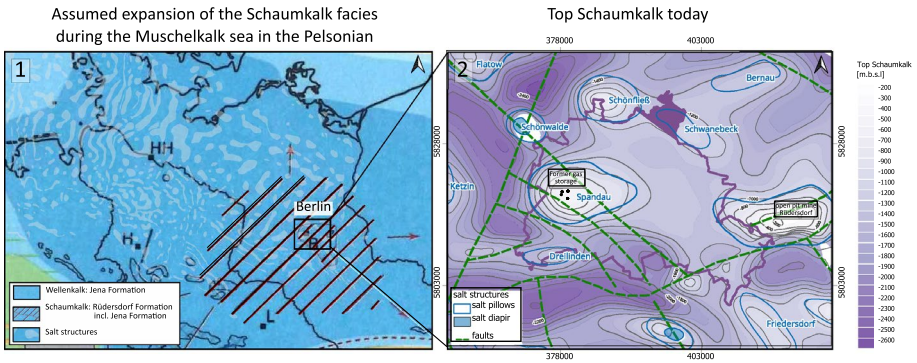

Fig. 1 (1) Map of salt structures in the North German Basin (data from BGR et al. (2022) and Tarkowski and Czapowski (2018) combined with the assumed lateral distribution of the Rüdersdorfer Schaumkalk (edited after Franz et al. (2020)). (2) Map displays the top of the Schaumkalk within the Berlin study area (data from Thiem et al. (2023))

Formation Schaumkalk has a total thickness of up to 73 m (Zwenger & Koszinski 2009). The Schaumkalk, a medium- to thick-bedded limestone with over 90% $CaCO_3$, is typically characterized by beds with dissolution pores formed by the dissolution of ooids (Kramm and Hagdorn 2021; Noack and Schroeder 2003; Zwenger and Koszinski 2009). Its presumed distribution extends from the Oderbruch to the Lusatia and from western Brandenburg to Lower Silesia (Hagdorn et al. 2021). Halokinetic movement of the Zechstein salts began in the Middle Triassic, intensified during the Jurassic, and continued in the Late Cretaceous (Zhang et al. 2013). This movement lifted the Muschelkalk in Rüdersdorf to the surface. Meanwhile, in Spandau, the Schaumkalk formation is found at depths of 400 m below sea level after the uplifting of the Spandau salt pillow, on which the former gas storage was constructed.

While reports of karstification are documented at a drilled well in Buchholz-Beelitz, located around 40 km southwest of the study site, where the Schaumkalk is not overlain by other Mesozoic rocks, such phenomena were not observed in the Spandau cores or the Rüdersdorf pit mine. In the context of the North German Basin, the entire Muschelkalk formation has been described as an aquitard (Cherubini et al. 2014; Frick et al. 2022; Göthel 2016). However, notable losses of drilling fluid were observed within the Schaumkalk layer in Spandau during the drilling of gas storage wells (NLfB 1989). Furthermore, the production tests that followed yielded formation water (NLfB 1989).

In Spandau, the Rüdersdorf Schaumkalk forms a fractured aquifer that is exposed at several wells of the former Berlin natural gas storage facility. Between 1992 and 2017, natural gas was stored in the underlying porous sandstone aquifer of the Bunter. After the separation of gas and fluid, the produced brine was injected into the fractured Schaumkalk aquifer, located 300 m above. Wells (BH01–BH03) were drilled for this purpose and perforated at the depths between 514 and 586 m MD (measured depth). Due to intermittent operation and injection, the exact amount of injected fluid cannot be specified. However, a total of at least 6900 to a maximum of 35,800 m^3 fluid was injected in the Schaumkalk during the gas storage operation from 1991 to 2015. And at least 1700 m^3 of Bunter formation fluid were injected into BH03 and 680 m^3 into BH02 in the last 4 years of operation. No water was injected into the Schaumkalk from the newly cemented and perforated former production well B14, according to the operation

data from the company. The aquifer is separated from overlying freshwater formations by aquitards of mudstone and evaporites such as the tertiary Rupelian Clay with up to about 300 m thickness in total. Underlying the Schaumkalk, mudstones of the Sollinger sequence, the Röt Saline and clay as well as the dense deposits of the Wellenkalk formation separate the aquifers to the Bunter. The dismantling of all wells has been taking place since 2021.

Hydraulic testing

Hydraulic tests were carried out in three wells: Besides the former injection wells BH02 and BH03, the former gas storage well B14, which was recently refilled to the Schaumkalk and perforated, was tested (Fig. 2). The tests were divided into two phases: Initially, slug-withdrawal tests were performed in all wells. Based on these results, BH02 was not considered further. In 2020, a total of 53 m^3 water was produced during a nitrogen lift test with flow rates up to 3.8 m^3/h from well B14. The flow rates generated a maximum drawdown of 28—30 bar (Blöcher et al. 2023). The performance index of the well exhibited a significant decline, mirroring the decreasing flow rates, and decreased from approximately 0.05 L/s/bar at the beginning of the lifting process to values around 0.02 L/s/bar at the end of the pumping phase (Blöcher et al. 2023). In 2021, a total of 39 m^3 of

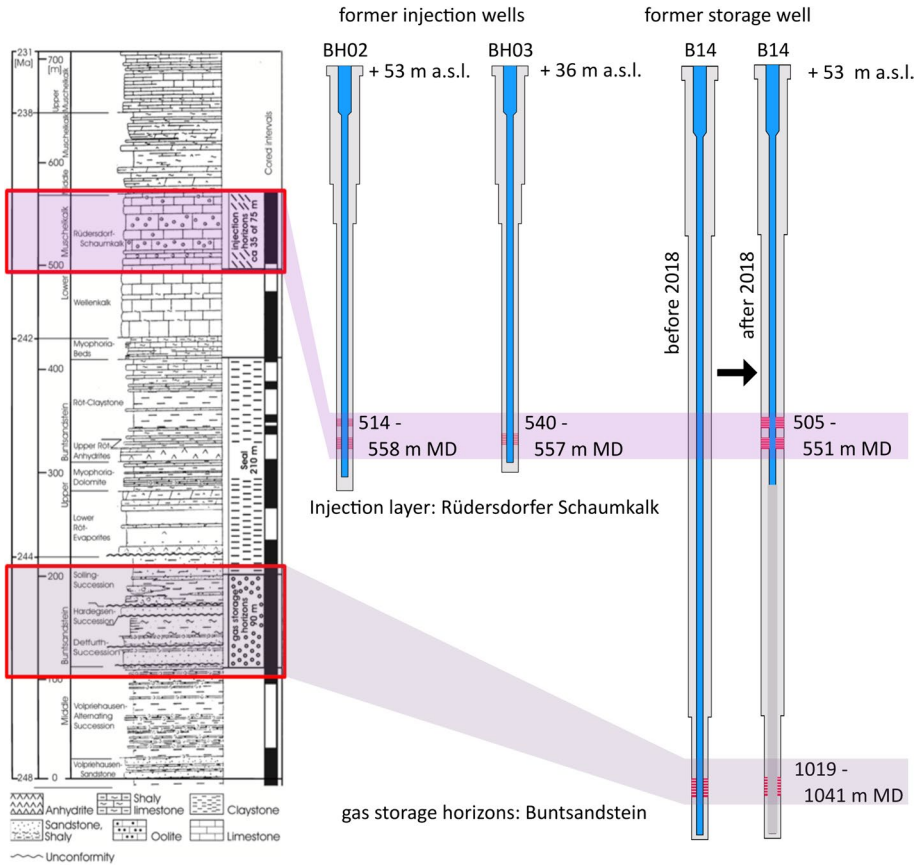

Fig. 2 Stratigraphy of the study site (edited after Noack and Schroeder (2003)) and the tested wells BH02, BH03, and B14

groundwater was produced from BH03 during a step rate test consisting of five stages, as well as a 16 h production test utilizing pump rates ranging from 0.5 to 2 m^3/h, followed by an injection test. From the step rate test, an initial productivity index of 8 to 9 L/s/bar was determined. The calculated injectivity index/performance index started at approximately 10 L/s/bar and decreased to around 2.5 L/s/bar by the conclusion of the injection test (Blöcher et al. 2023).

Gas sampling—wellhead

In May 2021, the wellhead gas was sampled at BH02 and BH03. The gas was fed from the wellhead into gas sample devices with a hand pump, and the composition and the $\delta^{13}C$ isotopes were subsequently determined via gas chromatography and quadrupole mass spectrometry.

Gas sampling—downhole sampling

Downhole fluid samples were collected using a Leutert Positive Displacement Sampler (Regenspurg et al. 2010). Sampling took place before and after the hydraulic tests at approximately 510 m and 526 m MD under in situ pressure and temperature conditions in the upper part of the BH03 perforation. Two other samples were taken after the tests at B14 (510 m MD) and BH02 (510 m MD). After each downhole fluid sampling, the samples were transferred into storage cylinders, maintaining the in situ pressure.

Gas–water separation of the downhole fluid samples and thus determination of the gas quantity and water–gas ratio took place at GFZ laboratories, following protocols described in Feldbusch et al. (2018) and Wiersberg et al. (2004). The separated gas samples provide information on absolute gas concentrations (i.e., the amount of gas dissolved in a given volume of formation water), gas composition, $\delta^{13}C$ isotopes, and yield information about possible changes due to the hydraulic tests.

Gas monitoring

The gas monitoring was carried out on a bypass during the production test at BH03 (Fig. 3). Here, the produced water passed through a degasser, where the gas was subsequently routed directly into the quadrupole mass spectrometry. In addition, five gas samples were taken during monitoring, which were analyzed for composition and $\delta^{13}C$-methane isotopes.

In situ measurements and fluid monitoring

Water sampling and physicochemical monitoring were carried out during the hydraulic tests of the B14 and BH03 at a bypass of the production line (Fig. 3). To ensure a continuous flow even in case of a blocked filter, two filter units with a mesh size of 60 µm were connected in parallel upstream of the measuring electrodes. In the flow-through measurement cell, the pH value, the specific electrical conductivity (EC) and temperature, the dissolved oxygen (DO) and the oxidation–reduction potential (ORP) were measured by probes over the entire test period and recorded every 20 s. The flow rate within the

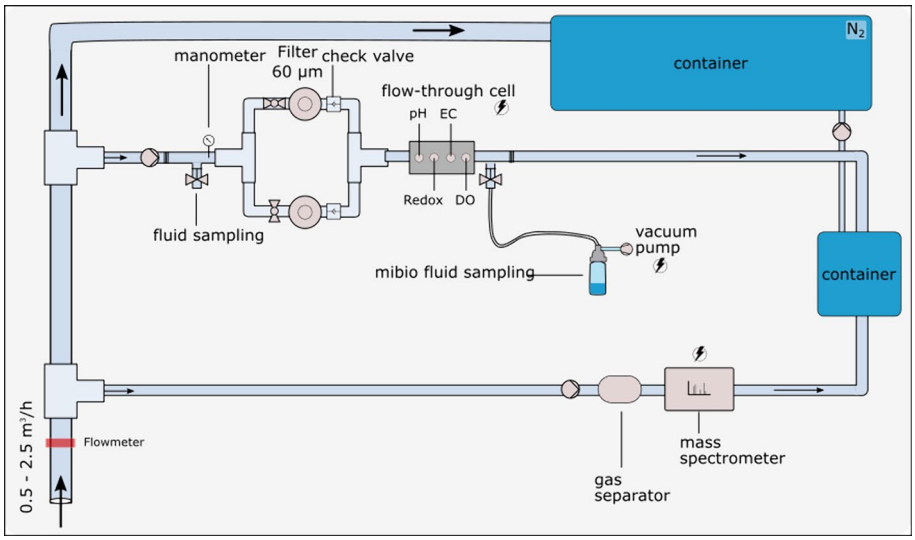

Fig. 3 Experimental setup of the field monitoring allowing the online monitoring of various physicochemical parameters and collection of gas and water sample in a bypass

bypass was approximately 0.6 L/min. Figure 3 shows the experimental setup at the well test site incl. the flow scheme, the flow-through cell, and sampling points.

For the analysis of inorganic ions, 2 × 15 mL of water sample was filtered through a 0.45 µm cellulose acetate membrane disposable filter and filled to the brim in sterile polypropylene tubes. An additional 10 µL of 2 M HNO_3 was added to the samples for cation analysis, adjusting the pH to < 2, to prevent potential precipitation of elements upon contact with oxygen. Samples for anion analysis were not further preserved. After sampling, the sample bottles were stored in a dark and cool place until analysis to prevent photodegradation. In addition, the acid binding capacity K_a 4.3 (carbonate hardness) was determined by means of a titration rapid test. For this purpose, three drops of orange methyl indicator were added to 5 mL of water sample. The solution was then titrated with hydrochloric acid to a pH of 4.3, which was evident from a color change. Other non-conservable ions such as sulfide and silica were also determined immediately after sampling at the well site using a filter photometer. The density was determined for each sampling with a portable density meter.

Water analysis

The inorganic anions were measured by ion chromatography (IC) and cations by inductively coupled plasma-optical emission spectrometry (ICP-OES). In addition, the last fluid sample of each test was analyzed for the $\delta^{34}S\text{-}SO_4$ [‰V-CDT] isotope by isotope ratio mass spectrometry. The $^{87}Sr/^{86}Sr$ ratio was determined by thermal ionization mass spectrometry and the stable isotopes δ^2H and $\delta^{18}O$ by isotope ratio mass spectrometry (TC/EA-IRMS). All water sample analyses of the hydraulic tests have an ion balance error of < 2%. Furthermore, a selection of water samples was analyzed for organic components like organic acids, dissolved organic carbon (DOC), and total organic carbon (TOC) via TOC Analyzer.

Microbiological characterization

During the hydraulic tests, water samples were taken periodically and filtered on site via vacuum pump. Immediately after filtration, the filters were placed in containers with liquid nitrogen and taken to the laboratory. In a laminar-flow cabinet, the filters were subsequently placed in the reaction tubes of the Power Soil pro DNA-extraction kit (Qiagen, Hilden Germany). DNA was extracted according to manufacturer protocol, and it was quantified with a Qubit 2.0 device following the dsDNA HS assay (Thermo Fisher scientific, Waltham Massachusetts).

Bacterial and archaeal 16S rRNA gene fragments were PCR amplified in triplicates and barcoded with primers 515F and 806R (EURx, Gdansk, Poland). The final volume of the reaction mixture was 50 µL, containing 2 µL of DNA template, 0.5 µL of Taq DNA polymerase, 2 µL of dNTP mix and $MgCl_2$, 5 µL of 10xC, 0.5 µL BSA, 2.5 µL of primers, and 35.5 µL of PCR water. PCR amplifications were performed using 5 min of initial denaturation at 95 °C, followed by 32 cycles of 30 s at 95 °C, 30 s at 56 °C, and 1 min at 72 °C. The final extension step was at 72 °C for 7 min. The PCR products were cleaned up with magnetic beads (AMPure, Beckman Coulter, Brea, California), and the samples were pooled.

All the PCR products were pooled equally in a final concentration of 20 ng for paired-end sequencing (2×300 bp) on Illumina MiSeq (Eurofins Genomics Europe Sequencing GmbH, Constance, Germany).

The sequencing library was demultiplexed using cutadapt v3.4 (55) using the following parameters:—e 0.2 -q 15,15 m 150—discard-untrimmed identifying only read pairs with correct barcodes at both ends. The ASVs were generated using trimmed reads and the DADA2 package v1.20 (56) with R v4.1 using the pooled approach with the following parameters: truncLen = c(240,200), maxN = 0, rm.phix = TRUE, minLen = 200. Taxonomic assignment was done using DADA2 and the SILVA database v138 (57). Subsequently, ASVs representing chloroplasts, mitochondria, and singletons were removed.

Solid phase analysis

Mineralogical analyses were performed on powder samples using a PANalytical Empyrean X-ray powder diffractometer (XRD). The sample material was crushed with a jaw crusher and subsequently powdered with a ball mill to a grain size of < 62 µm. To gain a most accurate random distribution of the powdered sample, it was loaded from the back side of the sample holder. Analyses were performed using the Bragg–Brentano geometry at 40 mA and 40 kV with CuKα radiation, and a PIXel3D detector at a step size of 0.013° 2theta from 4.6° to 85° 2theta and 60 s per step. The mineralogy was determined with the software EVA (version 11.0.0.3) developed by Bruker Corporation.

Geochemical model description

Hydrogeochemical modeling was carried out using PhreeqC Version 3.7.7.15968 (Parkhurst and Appelo, 2013). Based on high salinity and good correlation between calcite reactions with temperature variation, the pitzer.dat database was applied (Hörbrand et al. 2018). Inverse modeling simulates a possible evolution of the sampled formation

water using modern seawater (Mackenzie et al. 2024) and Triassic seawater (Horita et al. 2002) as the initial solution and the mean value of the sampled water from BH03. Evaporation was modeled by forcing $H_2O(g)$ precipitation with formation of gypsum ($CaSO_4 \cdot 2H_2O$). The model was extended to account for potential dolomitization associated with gypsum formation (Chen et al. 2023). In addition, a reaction with calcite as the surrounding aquifer material was allowed. Uncertainties for the model were set up to 5%.

For HT-ATES equilibrium modeling, the influence of temperature increases on the thermodynamic equilibrium during operation was computed. Input parameters included data from water and gas sample analyses (concentrations and volumes) and XRD analyses of drill core material from the porous Schaumkalk layers. The geochemical ATES modeling considered both open and closed CO_2 systems, pressure changes in the aquifer and at the surface, as well as temperature increases and decreases in the heat exchanger and partial temperature differences in the aquifer. The CO_2 partial pressure measured by the downhole samples was calculated as a function of depth and pressure conditions and was, thus, included in the calculation. Depending on the duration of ATES operation, temperatures were determined based on the hydrothermal storage simulation by Wenzlaff et al. (2022) (Fig. 4). The step-by-step procedure for calculation the chemical equilibrium during HT-ATES operation is described below. The temperatures for subsequent cycles are shown in Fig. 4:

Step 1—Initial solution.

The average of the BH03 water composition was equilibrated with the mineral phases as detected by XRD and the pCO_2 measured in the downhole samples to obtain the initial reservoir water composition.

Step 2—Charging the hot reservoir.

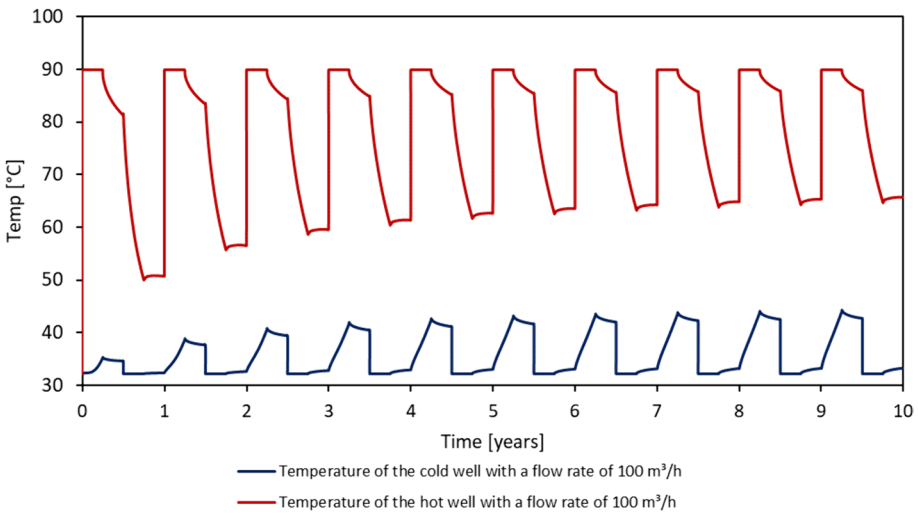

Fig. 4 Temperature cycles used for geochemical modeling of a carbonate HT-ATES and simulated for a 10 year production-injection period (data taken from Wenzlaff et al. (2022))

The water is produced from the so-called "cold reservoir " to the surface through the production well. At the bottom of the production well, the water has a temperature of 32 °C (= reservoir temperature) and a pressure of 57 bar (= reservoir pressure). As it is pumped to the surface, the pressure decreases to 5 bar (minimum assumed technical surface pressure). During production, the pressure in the reservoir decreases up to Δ 20 bar. It is further assumed that crystallization nuclei are present in the water and that only mineral precipitation can occur in this step. Since the kinetics of calcite solubility in particular are very fast, possible precipitation products were allowed to be deposited immediately. The water flows through the heat exchanger, where the water is heated up to 90 °C in one model step. Afterward, the water is injected through the injection well into the "hot reservoir". At the surface, the water temperature is 90 °C and the pressure is 5 bar. The pressure increases to 57 bar at the well depth (= reservoir pressure).

Step 3—Inactive phase (up to 3 months).

During the inactive phase, the water cools down. The longer the storage is in operation, the smaller this effect becomes (Fig. 4).

Step 4—Discharging the reservoir.

The hot water is produced through the well to the surface. At the lower edge of the production well, the water has a temperature of 83 °C (= new reservoir temperature, depending on year of operation and produced volume) and a pressure of 57 bar. As it is pumped to the surface, the pressure drops again to 5 bar. During production, the pressure in the reservoir decreases up to Δ 20 bar. The water flows through the heat exchanger where the temperature in the water is cooled down to 32 °C. It is then injected back into the cold reservoir. At the top of the well, the water temperature is 32 °C and the pressure is 5 bar. At the lower level, the water temperature is 32 °C. The pressure is 57 bar (= cold reservoir temperature and pressure).

Step 5—Inactive phase (up to 3 months).

Due to the interaction between the doublets, the reservoir temperature in the cold reservoir increases to 35 °C during the inactive phase, while the temperature in the hot reservoir decreases to 51 °C. The model continues with step 2 for cycle 2 of HT-ATES operation and adjusted temperatures.

Results

Geochemical characterization of solid, fluid, and gas phase

Characterization of the Schaumkalk reservoir rocks

Core samples from three drillings (BH1, B7, and B8) were analyzed for mineralogical composition by XRD. The results indicated that the cores consist to more than 96% of calcite with minor amounts of siderite, quartz, ankerite, and traces of clay (Table 1).

Hydrochemical composition of the fluid

The water samples taken during the two hydraulic tests fluctuated greatly in terms of physicochemical parameters in the first few hours after the start of the hydraulic test, before stabilizing after producing a single volume of the borehole. Aquifer temperatures

Table 1 Qualitative and quantitative X-ray diffraction results of BH1, B7, and B8. Mineral content is given in wt.-%

Formation	$Ca[CO_3]$	SiO_2	$Fe[CO_3]$	$CaFe[CO_3]_2$	$SrSO_4$			
	Calcite	Quartz	Siderite	Ankerite	Celestite	Clay	$^{87}Sr/^{86}Sr$	2 SE
Massive limestone, hanging layer	98.5	0.3	0.7	0.5		x		
Schaumkalk, upper porous layer	97.2	0.3	0.7	1.8				
Schaumkalk, upper porous layer	98.0	0	0.5	1.5	x		0.70781	0.000013
Massive limestone, inter layer	98.7	0.3	0.5	0.5		x		
Clayish limestone, inter layer	96.0	2.5	0.5	1.0				
Schaumkalk, lower porous layer	97.0	0	0.5	1.0	x		0.70781	0.000008
Massive limestone, foot layer	97.4	0.7	0.7	1.2		x		

were measured by Distributed Temperature Sensing and ranged between 31 and 34 °C. The pH stabilized in the slightly alkaline range around 7.7 in B14, while in BH03, it was slightly acidic with a pH of 6.3. The specific electrical conductivity varied between 150 and 180 mS/cm during monitoring. Due to partly inconstant flow and changes of the filter, the ORP did not reach stable values until the end of the tests whereby the lowest measurements were down to − 600 mV with an average of − 400 mV. Conversion to E_H shows reducing conditions with E_H values up to a minimum of − 300 mV. Density increased to 1.087 g/cm^3 as the tests progressed. Dissolved oxygen was continuously measured to be below 0.02 mg/L, confirming the oxygen-free sampling set up.

The sampled formation waters from both B14 and BH03 are very similar and highly saline with total dissolved solids (TDS) of about 130 g/L (Table 2 and Fig. 5). The dominant ions are sodium and chloride, accounting for 95% of the TDS. Calcium is the second most prevalent cation after sodium (43 to 48 g/L) with concentrations ranging between 3.2 and 3.7 g/L. Magnesium has less than half the concentration of calcium with values between 1.3 and 1.4 g/L. Potassium concentrations for both wells are at a level of 350 mg/L, strontium values range between 45 and 130 mg/L, boron concentrations are between 14 and 25 mg/L, and lithium concentrations range from 5 to 19 mg/L. On-site measurements show sulfide concentrations of up to 10 mg/L and silica values in the low single-digit mg/L range. Redox-sensitive components at higher concentrations are only detected at the beginning of the sampling by elevated iron concentrations (125 mg/L), decreasing and stabilizing at lower levels of about 0.4 to 0.03 mg/L. Manganese concentrations at the end of monitoring range from 0.3 to 0.04 mg/L in both wells. Besides the elevated concentrations of chloride (77 to 80 g/L), sulfate is notably present with concentrations spanning from 2.9 to 3.2 g/L. Bromide levels are found to vary between 240 and 280 mg/L, while fluoride concentrations are observed in the range of 1 to 3 mg/L. Field-measured alkalinity exhibits concentrations between 160 and 260 mg/L. Trace elements such as arsenic (< 0.03 mg/L), barium (< 1.4 mg/L), cadmium (< 0.03 mg/L), copper (< 0.5 mg/L), aluminum (< 0.006 mg/L), and zinc (< 1.0 mg/L) are detected, but only in trace amounts. After producing multiple volumes of the wells, the concentrations vary only slightly. Minor differences and variances in concentrations between the wells, as well as within the monitoring period, can be attributed to analytical scattering caused by high salinity. The analysis of the downhole samples agrees well with the monitoring

Table 2 Hydrochemical composition of the fluid in the three investigated wells targeting the Schaumkalk (B14, BH03, BH02) in comparison with the composition of Bunter formation (B15) fluid, that was occasionally injected into the Schaumkalk formation in the wells BH02 and BH03

		B14				BH03				BH02	B15
		Hydraulic test ($n = 13$)			DS	Hydraulic test ($n = 3$)			DS	DS	Production
		Min	Mean	Max		Min	Mean	Max			
Depth of Schaumkalk layer	[m MD]		505–551		510		540–557		510	510	–
Temp	[°C]		33				32			nan	nan
pH	[–]	7.0	7.7	7.8	nan	6.3	6.3	6.3	nan	nan	nan
E_H	[mV]	− 301	− 206	− 156	nan	− 125	− 115	− 92	nan	nan	nan
Density	[g/cm^3]	1.082	1.085	1.086	nan	1.086	1.086	1.087	nan	nan	nan
TDS	[g/L]	129	132	136	130	129	129	129	125	123	267
Boron	[mmol/L]	1.66	2.03	2.27	1.94	1.29	1.39	1.48	1.48	1.29	1.39
Barium		0.002	0.003	0.008	0.003	< DL	0.0004	0.0004	< DL	0.001	0.001
Calcium		77.4	84.6	92.3	87.3	90.3	91.2	92.1	89.3	82.8	394.2
Potassium		7.21	8.83	9.16	5.59	8.90	9.08	9.26	9.10	10.89	30.18
Lithium		1.37	1.77	2.71	0.58	0.69	0.70	0.71	0.68	0.71	2.85
Magnesium		51.5	55.2	59.5	53.5	54.3	54.7	55.1	53.9	51.0	54.3
Manganese		0.001	0.001	0.004	0.016	0.004	0.005	0.006	0.005	0.105	0.186
Sodium		1918	1980	2131	1827	1875	1881	1892	1870	1849	3480
Iron		0.001	0.002	0.011	0.154	0.008	0.011	0.015	nan	nan	nan
Silicium		0.057	0.113	0.132	0.173	< DL	0.285	0.285	nan	nan	nan
Strontium		0.512	0.532	0.584	0.493	1.108	1.263	1.529	0.945	1.026	8.092
Chloride		2161	2200	2313	2231	1810	2074	2181	2059	2051	4694
Bromide		2.33	2.96	3.18	nan	2.96	3.23	3.38	2.98	3.05	13.42
Sulfate		30.6	31.7	33.3	33.1	26.0	30.8	33.1	30.9	22.5	3.9
Fluoride		0.106	0.116	0.125	< DL	0.143	0.148	0.152	nan	nan	nan
Alkalinity		3.0	3.6	4.5	3.4	2.5	2.7	2.9	4.0	7.0	3.0
Sulfide		0.03	0.08	0.13	0.01	0.19	0.25	0.32	nan	nan	nan

Table 2 (continued)

		B14				BH03				BH02	B15
		Hydraulic test ($n = 13$)			DS	Hydraulic test ($n = 3$)			DS	DS	Production
		Min	Mean	Max		Min	Mean	Max			
Aluminum	[µmol/L]	0.030	0.105	0.193	0.148	nan	nan	nan	nan	nan	nan
Antimony		0.164	0.554	0.944	0.115	nan	nan	nan	nan	nan	nan
Arsenic		0.147	0.247	0.347	0.147	nan	nan	nan	nan	nan	nan
Cadmium		0.009	0.011	0.012	0.033	nan	nan	nan	nan	nan	nan
Copper		0.063	0.094	0.126	7.365	nan	nan	nan	nan	nan	nan
Zinc		3.105	3.579	4.053	31.202	nan	nan	nan	nan	nan	nan
TOC	[mg C/L]	19.9	25.0	31.9	nan	nan	nan	nan	nan	nan	nan
DOC	[mg C/L]	16	20.5	28	nan	6.01	6.22	6.62	nan	nan	nan
Acetate	[mg/L]	40.9	49.9	62.0	nan	1.13	1.20	1.26	nan	nan	nan
Propionate		< 1	< 1	< 1	nan	< 1	< 1	< 1	nan	nan	nan
Formiate		1.2	3.6	5.9	nan	< 1	< 1	< 1	nan	nan	nan
Butanate		< 1	< 1	< 1	nan	< 1	< 1	< 1	nan	nan	nan
$\delta^{34}S$	[‰]		20.9				21				nan
$\delta^{2}H$			− 36.44				− 35.95				− 28.57
$\delta^{18}O$			− 5.49				− 5.40				− 2.56
$^{87}Sr/^{86}Sr$			0.70788				0.70802				0.71002
2 SE			1.70E−05				1.10E−05				1.40E−05

Samples were either collected in the wellbore with the downhole sampler (m MD) or above ground at the well head

DS: downhole sample, nan: not analyzed, DL: detection limit

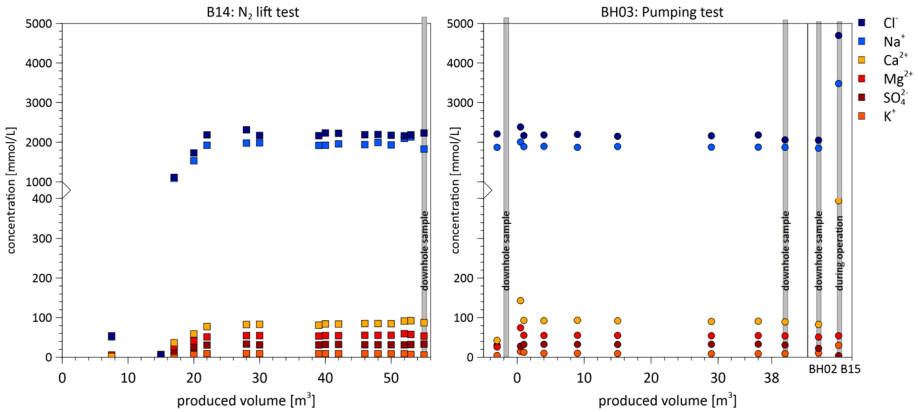

Fig. 5 Main ions measured in samples of the formation water of B14 (left) and BH03 (right), collected during the hydraulic tests, over cumulative produced volume. The right-hand graph also displays the major ions of BH02 and the Bunter formation water

results and confirms theses values with minor deviations. The downhole sample from BH02, which was not further subjected to hydraulic testing, also shows comparable concentrations. The two monitored wells display very similar inorganic components.

For comparison, one water sample from the former gas storage aquifer (Bunter formation), which has been injected into the Schaumkalk aquifer for more than 20 years, was also collected and analyzed. Comparison with the Schaumkalk formation water shows that the TDS is twice as high at 267 g/L, with sodium (80 g/L) and chloride (166 g/L) being the main ions followed by calcium with 15.8 g/L. Magnesium, boron, and barium are present at similar concentrations, while sulfate is present at a tenth of the concentration.

In the aqueous phase, $\delta^{34}S$, $\delta^{2}H$, $\delta^{18}O$, and $^{87}Sr/^{86}Sr$ were measured in samples from B14, BH03, and from fluid of the Bunter formation (B15). Results indicate similar values in the BH03 and B14 of $\delta^{2}H$ (− 35.9 to − 36.4), $\delta^{18}O$ (− 5.49 to − 5.40) (Table 3), and $^{87}Sr/^{86}Sr$ (0.70788 to 0.70802, Fig. 6) which differ strongly from the B15 sample (Table 2). In the Schaumkalk rock, $^{87}Sr/^{86}Sr$ is 0.70781. A plot of the measured $^{87}Sr/^{86}Sr$ ratios of rock and water as well as in comparison to Triassic (Burke et al. 1982) and modern sea water is given in Fig. 6. A similar result was obtained from the sulfate isotope analysis $\delta^{34}S$ of the most recently collected water samples of each monitoring session that exhibit a similar signature of 20.9 and 21.0 ‰, respectively.

Chemical composition of the dissolved gases

The total volume of dissolved gases was generally low in the two samples from BH03 and the sample from B14 with values typically around 30 mL/L at standard temperature and pressure (Table 3). An exception is the gas content in well BH02 with gas concentrations of 164 mL/L. In well BH03, downhole and wellhead sampling before and after well testing was accompanied by an extensive gas monitoring performed during the outflow test. Whereas for BH02, only two samples were collected (one wellhead and one downhole fluid sample) and for B14, only one sample was taken (collected with the downhole sampler).

Table 3 Chemical composition of gases of the three investigated wells targeting the Muschelkalk (B14, BH03, BH02)

Well		B14	BH03	BH03	BH03[a]	BH03[a]	BH03	BH03	BH03	BH03	BH02	BH02
Info		510 m MD	Wellhead	538 m MD	Surface monitoring					526 m MD	Wellhead	510 m MD
Volume	[mL/L]	28.45	–	32.94	20	–	–	–	–	32.53	–	164.07
Ar	[vol.-%]	0	0	1.11	0.9	0.8	0.6	0.6	0.8	1.11	–	0.337
CO_2	[vol.-%]	53.5	0.1	0.388	0.05	0.05	2.6	1.3	2.6	1.75	0.013	0.3075
H_2	[vol.-%]	26.6	3.4	0.068	–	–	0	0	0	0.085	4.2	0.196
O_2	[vol.-%]	–	5.35	–	18.8	18	5.1	3.8	0.2	–	1.35	–
N_2	[vol.-%]	–	88.3	81.06	78.5	78.3	61.4	63.5	66.8	66.8	62.6	32.16
He	[vol.-%]	–	–	0.7545	< 0.05	< 0.05	< 0.05	0.9	1.5	0.719	–	0.1424
CH_4	[vol.–%]	19.8	2.6	16.6	1.1	2.8	29.9	29.5	28	29.5	29	67
C_2H_6	[ppmv]	800	500	1080	83	245	254	344	129	–	6000	915
C_2H_4	[ppmv]	500	–	36	–	–	–	–	–	–	0	85
C_3H_8	[ppmv]	300	100	380	91	145	425	477	267	–	1100	25
i-C_4H_{10}	[ppmv]	100	20	60	49	42	187	199	152	–	210	170
n-C_4H_{10}	[ppmv]	100	2	155	106	98	455	464	377	–	180	460
i-C_5H_{12}	[ppmv]	–	–	–	109	174	501	699	496	–	–	–
n-C_5H_{12}	[ppmv]	–	–	–	76	124	395	466	367	–	–	–
δ^{13}C-CH_4	[‰]	–	− 55.03	− 61.311	− 53.4	− 56.2	− 62.2	–	− 59.8	–	− 70.79	− 62.764
δ^{13}C-CO_2	[‰]	− 15.44	− 16.02	− 24.131	–	–	–	–	–	–	− 15.17	− 25.521
$C_1/(C_2+C_3)$	[–]	–	42	97	21	34	135	111	157	–	39	326

[a] Large influence of the atmosphere while sampling

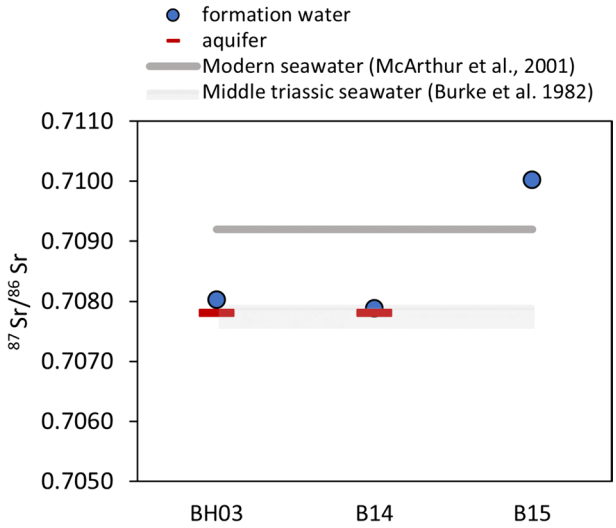

Fig. 6: $^{87}Sr/^{86}Sr$ ratio in the water samples BH02 and B14 as well as in the Muschelkalk (Schaumkalk) rock. For comparison, modern seawater (McArthur et al. 2001) and Triassic seawater (Burke et al. 1982) are plotted

The dominant gas in BH03 and BH02 is nitrogen with values between 81 and 88 vol.-% before and 67 vol.-% after well testing, followed by methane roughly 17 vol.-% before well testing and 29 vol.-% thereafter. Comparing headspace gas from the wellhead of BH03 with gas from downhole fluid sampling from BH03 shows higher concentration of N_2 at the wellhead (88 vol.-%) compared to the downhole (81 vol.-%). A similar observation is also made in BH02 (63 to 32 vol.-%). Wellhead gases are generally enriched in N_2 and H_2 and depleted in CH_4, compared to their downhole counterparts, due to the higher solubility of CH_4 in water, compared to N_2 and H_2. Over the time of the outflow test in BH03, methane increases and nitrogen decreases, and the gas composition of the produced fluid becomes more and more similar to the composition of the downhole sample, dominated by N_2 (67 vol.-%) and CH_4 (28–30 vol.-%). Only the sample from BH02 collected with the downhole sampler showed a strong domination of methane (67 vol.-%) over nitrogen (32 vol.-%; Table 3). The downhole sample B14 differed even more strongly from BH02 and BH03, because here CO_2 was the dominant phase (54 vol.-%) and also high hydrogen content was measured (27 vol.-%). In the aquifer, pressure conditions of 57 bar prevail, leading to the assumption that the gases measured here are dissolved in the water.

Microbial and organic carbon analysis

Sequencing results indicate a diverse microbial community in the formation water, predominantly comprising sulfate-reducing bacteria (SRB) and methanogenic archaea. A significant portion of the identified taxa exhibits halophilic traits. The most dominant SRB at the two sites are represented by the genera *Desulfosalsimonas* for the site B14 and *Desulfovermiculus* for the site BH03 (Fig. 7). Methanogenic taxa at the site BH03 primarily belong to the order *Methanofastidiosales* and the genus *Methanohalophilus*. Conversely, at the site B14, the prevailing genus among methanogens is *Methanobacterium*. Site BH03 exhibited minimal variation in the microbial community across the 2 days of sampling. In contrast, site B14 demonstrated a shift in microbial composition within the

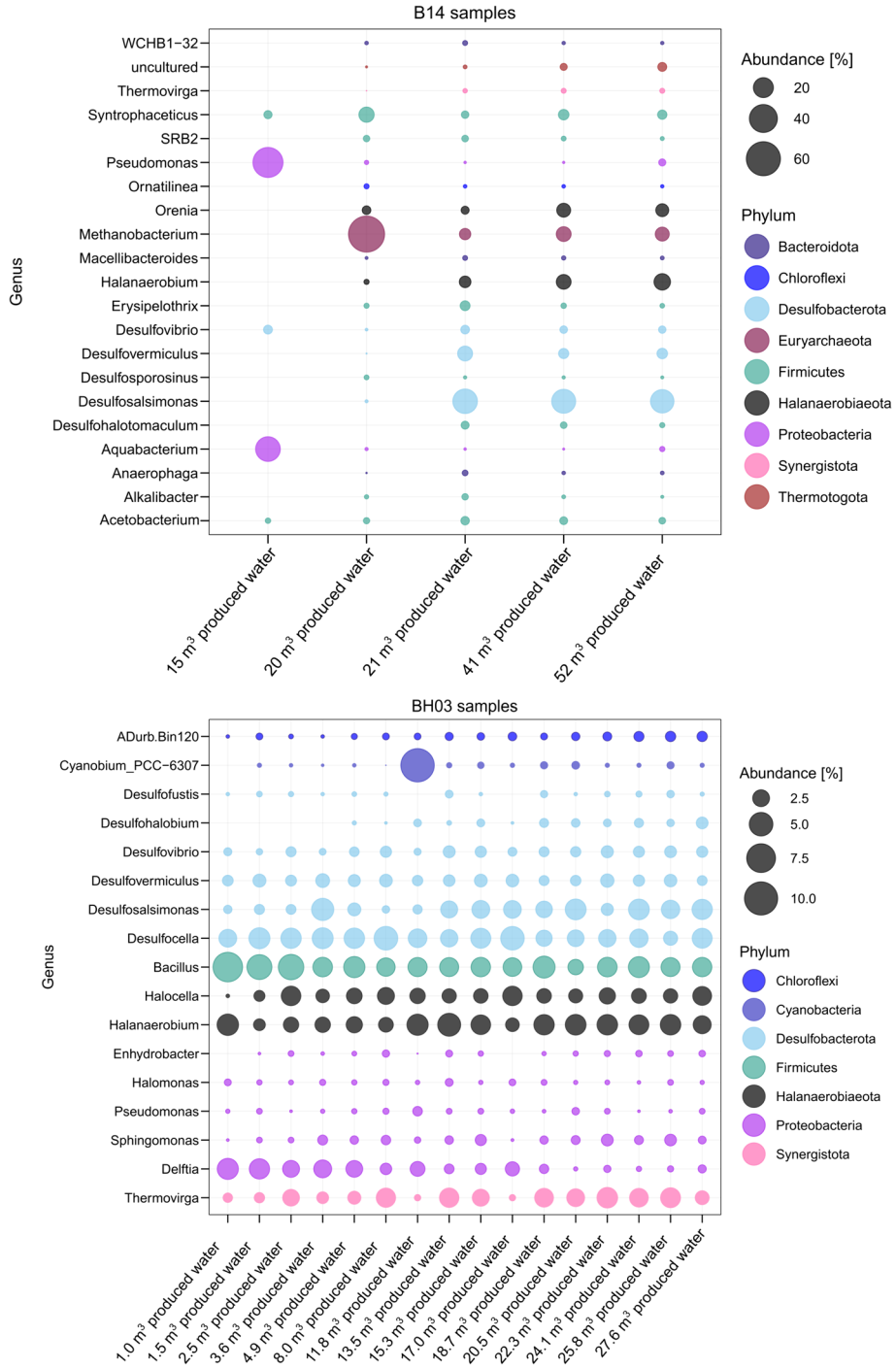

Fig. 7 Overview of abundance, genus, and phylum of detected microorganisms in the samples from B14 with 95% of the total taxa (top) and BH03 with 92% of the total taxa (bottom) collected over cumulative produced volume

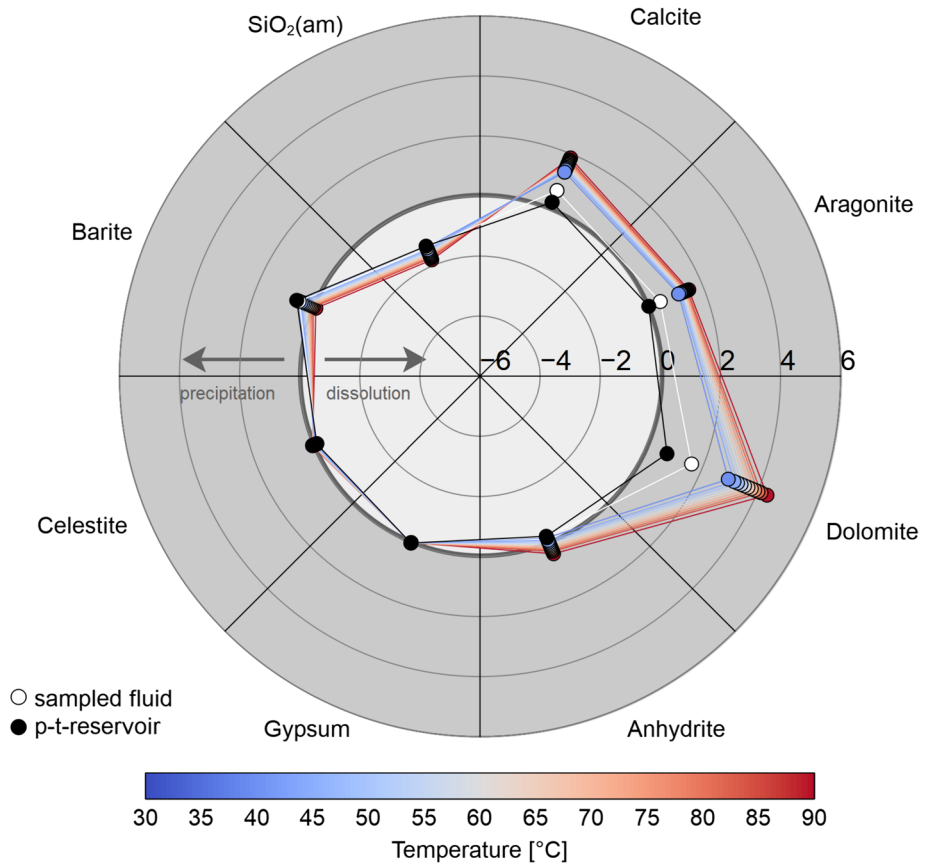

Fig. 8 Calculated SI at the heat exchanger with increasing temperature (32–90 °C). The measured p–t conditions at the reservoir were 56 bar, 32 °C, and a pCO_2 of − 1.54 atm. To take into account the lower CO_2 solubility due to the pressure reduction, the pCO_2 at the heat exchanger is set to − 2.3 atm

initial 1.5 h of pumping, subsequently stabilizing and maintaining consistency over the ensuing 24 h. Overall, the observed microbial composition suggests that the formation water at both sites is consistently anaerobic and contains dissolved salts. The DOC and the organic acid acetate show a similar behavior (Table 2): They increase in the beginning and decrease with acetate concentrations stabilizing at 40 mg/L in B14 and 1 mg/L at BH03 (Table 2).

Results of HT-ATES simulation

Geochemical modeling was performed based on the formation water from well BH03. The saturation indices presented here (Fig. 8) were calculated with respect to the changing equilibrium in the heat exchanger and are based on the site-specific measurements of temperature and pCO_2. With an initial temperature of 32 °C, the pressure at the heat exchanger is set to 5 bar, resulting in an initial pCO_2 of − 2.3 atm.

Critical mineral phases are carbonates and the calcium sulfate anhydrite, i.e., especially those with retrograde solubility. While the carbonates are supersaturated with respect to the fluid at reservoir conditions, the sulfates are in equilibrium. However, their saturation indices, SI all increase with increasing temperature. This indicates that these mineral phases have the potential to precipitate. Celestite is close to

equilibrium with minor changes with temperature. Barite is slightly supersaturated, but its saturation decreases with increasing temperature. Amorphous SiO_2 stays undersaturated with respect to the fluid (Fig. 8).

Discussion

Processes in the wellbores and origin of the well water

Mixing by injection of non-Muschelkalk brines and evaporation of seawater

The wells BH02 and BH03 were originally used during gas storage as injection wells for the residual brine from the Bunter sandstone after the gas was removed from the reservoir. Till 2015, at least 6900 m^3 brine from the Bunter (possibly contaminated with traces of storage gas) were injected into the Muschelkalk reservoir. This means, a mixing of the Bunter water with the original Muschelkalk formation water can be expected. In addition, those wells were occasionally used for injection of other fluids (tap or raw water) over the years of well operation, thus resulting in a complex mixing scenario. In well B14, other processes can be expected: this well was originally targeting the Bunter horizon, but recently backfilled with cement and perforated in the Muschelkalk horizon. After the recent drilling, tap water was injected into the well for cleaning purposes. Indeed, the first samples are a mixture of formation water and recently injected fluids, consisting of tap water after cementation of B14 and brine from the Detfurth well B15.

A variety of geochemical methods, including comparison of isotopes, ion ratios, and genesis pathways, were used to determine whether the produced water was primarily from the former Bunter water or the Muschelkalk reservoir.

It is evident that the brine previously injected for years was not solely produced during the recent production tests. The total salinity of the freshly produced water is about 130 g/L, whereas the salinity of the brine from the Buntsandstein is more than twice as high. Assuming that chloride behaves conservatively in a mixture, 55% of the Bunter Formation water would have to be mixed with water of very low salinity to achieve the chloride levels measured here. When the waters are mixed, a new chemical equilibrium

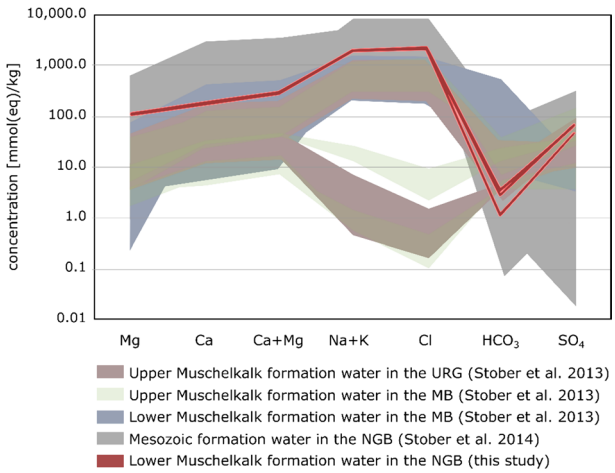

Fig. 9 Muschelkalk formation water from the URG and MB as well as Mesozoic formation water from the NGB presented as shaded patterns in a Schoeller diagram (data taken from Stober (2014); Stober et al. (2013) and this study)

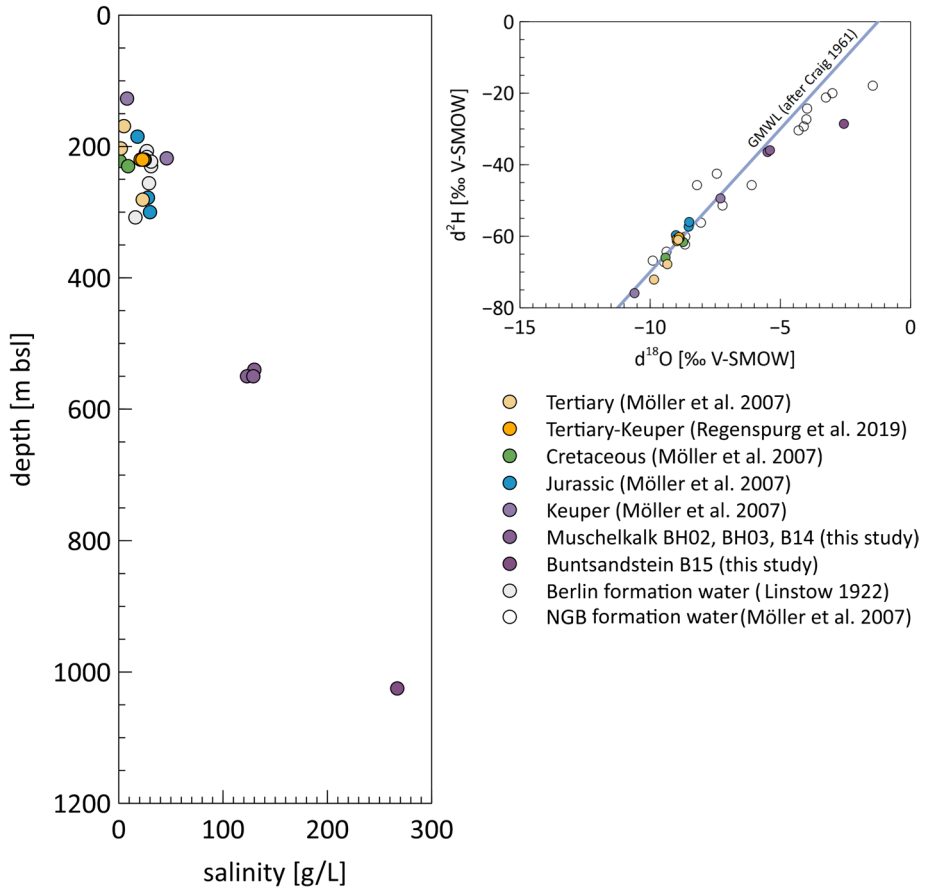

Fig. 10 left: plot of salinity versus depth of known pre Rupelian formation fluids from the study area Berlin (data taken from Linstow (1922); Möller et al. (2007); Regenspurg et al. (2019) and this study), right: plot of δ^2H and $\delta^{18}O$ of measured samples compared to various data from literature of fluids from the North German Basin and the Global Meteoric Water Line after Craig (1961)

may be established and calcite may precipitate, resulting in lower calcium concentrations, which could explain the lower calcium concentration in the mixing ratio. However, the large difference in sulfate concentration, which is ten times (mass ratio) higher in the formation fluid produced here than in the Bunter water, would remain unexplained.

A comparison with the literature shows that the deep Mesozoic formation waters from the North German Basin, the Upper Rhine Graben (URG), and the Molasse Basin (MB) have a similar composition, which is highly mineralized with sodium and chloride as the main ions (Fig. 9). Generally, the salinity of Mesozoic formation waters increases roughly linearly with depth in the North German Basin (Stober et al. 2014). In the salinity versus depth diagram (Fig. 10), also the overall salinity fits to the expected salinity of a formation water occurring at a given depth. The data collected in this study follow this line and plot between the Keuper samples and the Bunter samples (Fig. 10) indicating that the collected waters from the three wells B14, BH02, BH03 belong predominantly to the Muschelkalk formation water.

Water isotopes (δ^2H and $\delta^{18}O$) also suggest a predominant contribution of the Muschelkalk formation water to the samples collected in this study, as they all lie close to the global meteoric water line (GMWL) (Fig. 10). Mesozoic fluids measured across

the NGB likewise fall on the line (Möller et al. 2007; Regenspurg et al. 2019). In contrast, the Bunter (Detfurth) formation sample, which has a much higher salinity, indicates a stronger evaporation and further water–rock interaction, as implied by the shift away from the GMWL.

The most compelling argument indicating that the water analyzed from wells BH02, BH03, and B14 is significantly influenced by the Schaumkalk formation comes from the ratios of the $^{87}Sr/^{86}Sr$ isotopic data. The brine values range between 0.70788 (B14) and 0.70802 (BH02; see Table 2), closely mirroring the ratios found in the Schaumkalk rock sample (0.70781). In contrast, the Bunter brine has a markedly different isotopic signature of 0.71002 (Fig. 6). The values associated with the solid phase of the Schaumkalk and its corresponding formation water are also consistent with the isotopic range of ancient Triassic seawater (Burke et al. 1982; Korte et al. 2003), thereby strongly suggesting the origin of the formation water from the Muschelkalk or its significant influence on the fluid. Similarly, the sulfur isotopes show a signature distinctly influenced by the Middle Triassic. Comparisons with the sulfur isotope values reported by Bernasconi et al. (2017) and Kampschulte and Strauss (2004) for the Middle Triassic Anisian stage (about 21.5‰) reveal that these isotopes fall within the range characteristic of the Muschelkalk.

Figure 11 plots the various ion concentrations against their corresponding chloride concentration for the collected samples and previously mentioned data and adds the evaporation pathway of seawater from Fontes and Matray (1993). The water samples collected and analyzed in this study are all on the seawater evaporation pathway in terms of Na–Cl and Br–Cl, with the Muschelkalk fluids close to the gypsum precipitation point. Magnesium, potassium, and sulfate are depleted with respect to the seawater evaporation path. Calcium, as the only major ion, is enriched, as are strontium and lithium. However, it is not only the Na/Cl ratio that indicates a seawater influenced fluid, but especially the Cl/Br ratios as well. For BH02 and BH03, these ratios are 298 and 286 (mass ratio), respectively, which is directly comparable to the characteristic value of 288 found in modern seawater (Stober et al. 2023). Although B14 has a slightly higher value of 320, the fluid can still be classified within the same group. In contrast, fluids with halite dissolution signature have Cl/Br ratios of > 2000 (Stober et al. 2023). The Ca/Mg ratio (in molar) can indicate whether the water is influenced by dolomite (< 2.2) or was primarily in contact with calcite during its genesis and flow (> 2.2) (Langmuir, 1971). The ratios of the water from all three Schaumkalk wells range between 1.5 and 1.6, indicating contact with dolomite rocks during genesis.

From here, the question arises how this seawater composition changed over time to result in the composition of the water in the reservoir. It is known that during the Muschelkalk period, an arid climate existed and the Muschelkalk Sea evaporated strongly (Franz et al. 2020).

The results of the inverse models indicate that seawater, both modern and Triassic, must be concentrated up to fourfold to produce the sampled BH03 formation water (Table 4). Using modern seawater as the starting solution, the evaporation process leads to gypsum precipitation of 0.0199 mol/kg water, while for Triassic seawater, the precipitation is only 0.0062 mol/kg. Along with gypsum precipitation, dolomitization can occur, with up to 0.0352 dolomite being removed from the solution. The model shows that the fluid tends to dissolve calcite, thus enriching the fluid with 0.0698 or

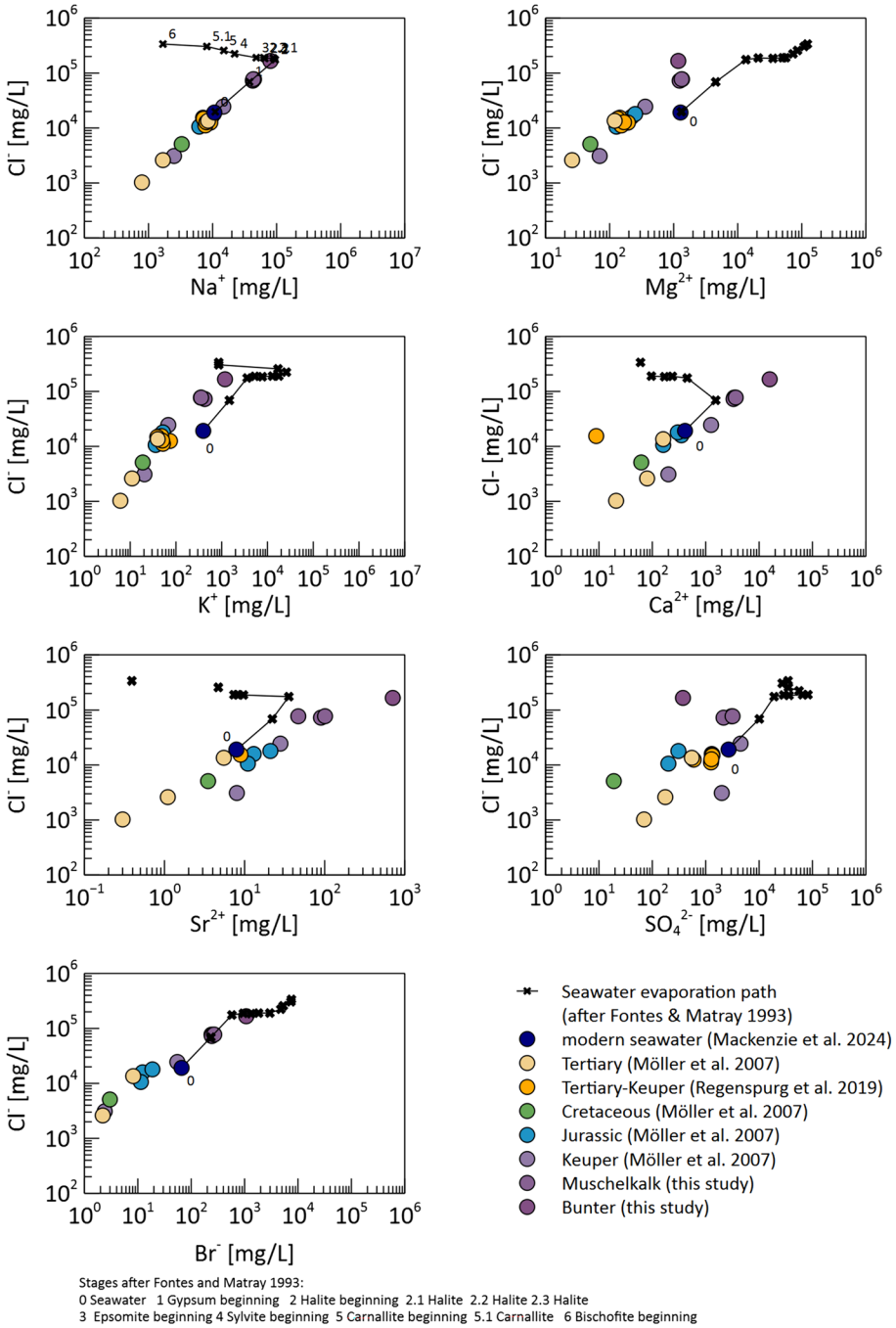

Fig. 11 Ion ratios plotted against chloride concentration including the seawater evaporation pathway (black dots and line) (data taken from Fontes and Matray (1993), Möller et al. (2007), Regenspurg et al. (2019) and this study)

0.0320 mol/kg calcite. Since the solution is not supersaturated with halite, the ions chloride, sodium, and bromide were declared conservative within the 5% uncertainty limit. The model shows that within the uncertainty range, evaporation, gypsum precipitation, dolomite formation, and the dissolution of calcite can explain the main ions found in the Schaumkalk formation fluid. Assumed processes are consequently

Table 4 The inverse modeling results show the amount of mineral phase transfer during possible fluid–rock reactions at evaporation of seawater

		Model 1	Model 2
Seawater		modern[a]	triassic[b]
Formation water		BH03	BH03
Concentration factor		4.0	3.9
$H_2O(g)$	[mol/kg water]	− 41.598	− 41.313
$CO_2(g)$	[mol/kg water]	− 0.0002	− 0.0002
Gypsum	[mol/kg water]	− 0.0199	− 0.0062
Dolomite	[mol/kg water]	− 0.0352	− 0.0162
Calcite	[mol/kg water]	+0.0698	+0.0320

[a] Data from Mackenzie et al. (2024)

[b] Data from Horita et al. (2002)

'−' removed, '+' added

(1) evaporation of the original seawater (Muschelkalk Sea) in the Mesozoic accompanied by gypsum/anhydrite precipitation and (2) hydrochemical transformation by water–rock interaction such as dolomitization resulting in a depletion of magnesium and enrichment of calcium in the water.

Geochemical alteration by corrosion and microbial processes

Besides mixing, other processes are expected to occur in the wells, such as corrosion and scaling, both of which can be induced or accelerated by microorganisms such as SRB. Signs of corrosion, potentially triggered by the elevated number of SRB, are notably evidenced by the elevated concentrations of H_2 gas in the wells. This is observed as a moderate rise in BH03 (3.4 vol.-%) and a significant surge in B14 (26 vol.-%), as detailed in Table 3.

The well B14 has to be considered differently as compared to BH02 and BH03, since this well was completed just shortly before the hydraulic tests by backfilling the well, originally targeting the Bunter horizon, with cement and perforating it in the Schaumkalk formation.

The higher pH value of the well (7.0–7.8) as compared to the other well, that shows a constant pH of about 6.3 (Table 2), confirms some impact of the relatively fresh cementation. The well B14 also showed a high concentration of dissolved iron in the beginning of the hydraulic tests (125 mg/L) that, however, quickly decreased to below 0.1 mg/L after pumping 10 m^3. Similarly, the high zinc content of 2 mg/L in B14 (as compared to 0.3 mg/L in all other samples) that was only measured in the downhole sample collected before the hydraulic test indicate a residue from perforation and corrosion (e.g., the use of galvanized casing). B14 also showed a very high content of CO_2 (53.5 vol.-%) as compared to the wells BH02 and BH03 (below 3 vol.-%, Table 2). This correlates with the high content of organic carbon (20–32 mg C/L) and, thus, points to a microbial degradation of the organic material that consists predominantly of acetate (50 mg/L), which also is often used by microorganisms as source of energy for their metabolism. However, the high organic content compared to other fluids from the NGB (Leins et al. 2022) could also be due to the operation of the former natural gas storage facility. The injection of residues from the storage gas and other organics cannot be excluded. As the Schaumkalk

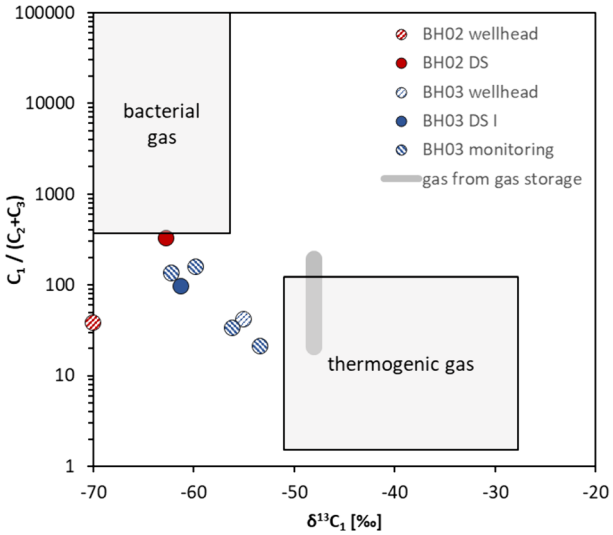

Fig. 12 Gas data plotted at a $\delta^{13}C_1$ versus $C_1/(C_2+C_3)$ diagram (after Bernard et al. (1976)). All samples fall between the two ranges of typical thermogenic and biogenic gas, indicating a mixture of the two. The storage gas is represented in gray and shows the ratios of the operation years

in B14 is topographically higher than the other injection wells, it could act as a geological trap and fluids with lower density, such as the lipophilic substances measured here, could accumulate and be measured in B14. Alternatively, residues from the cementation and perforation jobs (e.g., lubricating grease used for the cement injecting pipe) explain the high TOC content.

Another type of microbial process can be inferred from the methane content. Methane can either be of thermogenic or of microbial origin (Fig. 12). The methane content was between 20 and 30 vol.-% in most samples. Isotope measurements of $\delta^{13}C$ in CH_4 rank between − 55 and − 80 and thereby fall between the two ranges of typical thermogenic and biogenic gas, indicating a mixture of the two and a potential origin from both sources. The sample from BH02 collected with the downhole sampler contained even 67 vol.-% methane. This phenomenon may be due to increased microbial activity, as methanogenic microorganisms have been detected and the prevailing anoxic conditions are conducive to such processes (Fig. 7). A similar observation has been described in a former geothermal research well, where methane content strongly increased over 7 years of production stop (Regenspurg et al. 2024).

Evaluation of the performance of the site as a high-temperature ATES system

Fractured versus porous aquifer

In all three investigated wells, the water chemistry was similar and several indicators were found that the water collected derives predominantly from the Muschelkalk formation. This implies that most of the Bunter formation water that has been injected during the last 4 years of gas storage operation (2400 m^3) into the BH02 and BH03 wells "disappeared" from the vicinity of the wells (considering that only 39 m^3 have been pumped out during the tests). This indicates a strong flow of the injected water and, thus, that the water is predominantly transported in the reservoir via faults and fractures. The fact that

the Bunter formation water was exchanged by the Muschelkalk formation water is most likely caused by density differences since the Bunter water is more dense (approx. 1.18 g/cm^3) as compared to the Muschelkalk formation waters (1.082–1.087 g/cm^3; Table 2). This allowed the Bunter formation water to flow into deeper parts of the reservoir along the fractures system. Further indications for a high permeability of the formation are the high losses of drilling mud, when wells were drilled at the site through the Schaumkalk formation (NLfB 1989). Due to the location of the gas storage site on top of a salt diapir (Fig. 1), strong halotectonic processes can be expected as a result of the uplift of the Zechstein salt thereby inducing faulting of certain layers. Since the Schaumkalk has a very high porosity (Noack and Schroeder, 2003), given by the dissolution of the ooids in the oolithic limestone, the rocks are more brittle and might break more easily as compared to the surrounding more compact limestone formation.

The benefits of a fractured flow include increased permeability and capacity, which are conducive to ATES operations. Conversely, a vigorous flow could result in the displacement of the injected hot water, leading to its transportation along the flow path rather than remaining localized.

Calcite dissolution and precipitation processes in the HT-ATES during ten ATES cycles

Based on the saturation index from the chemical equilibrium calculations at elevated temperatures, PhreeqC simulations were carried out over ten ATES production and injection cycles. For these simulations, only calcite precipitation and dissolution were considered since this mineral is the dominant phase in the reservoir limestone rock and represents also the highest precipitation risk, as the changing parameters such as temperature and pCO_2, along with its presence in the aquifer, continuously create new chemical equilibria. In the model, calcite was assumed to be in equilibrium with the environment (either heat exchanger or aquifer) at each point after the temperature increase or decrease. This can lead to dissolution and precipitation within the ATES operation. Dolomite, on the other hand, is kinetically inhibited and is unlikely to precipitate under the given conditions (Chen et al. 2023).

Three locations in the fluid loop were selected for the equilibrium calculation: the hot reservoir (near the well bottom of the well where the hot water is injected and produced), the cold reservoir (near the well bottom of the other well used for injections of the cooled brine after heat extraction), and the heat exchanger, located above ground where the heat is removed from or added to the produced water of the hot or cold reservoir, respectively. For each cycle step (Fig. 4), the amount of calcite precipitation/dissolution of the heat charging phase, the resting phases, where no water is produced or injected, and at the heat exchanger were calculated (Fig. 13). Figure 13 illustrates the precipitation and dissolution potential of calcite during operation of a HT-ATES system. The charging and discharging phases refer to the hot reservoir. A temperature model was chosen in which the two reservoirs thermally influence each other. Therefore, even during the first charging phase, a temperature increase can lead to calcite precipitation of up to 7 mg/kg water in the cold reservoir. The greatest supersaturation occurs in the heat exchanger, where the water is heated to 90 °C. The water, previously in equilibrium with calcite, experiences an increase in saturation and as a result, 31 mg/kg water of calcite can precipitate in the heat exchanger. With a total water flow of 100,000 m^3 per cycle,

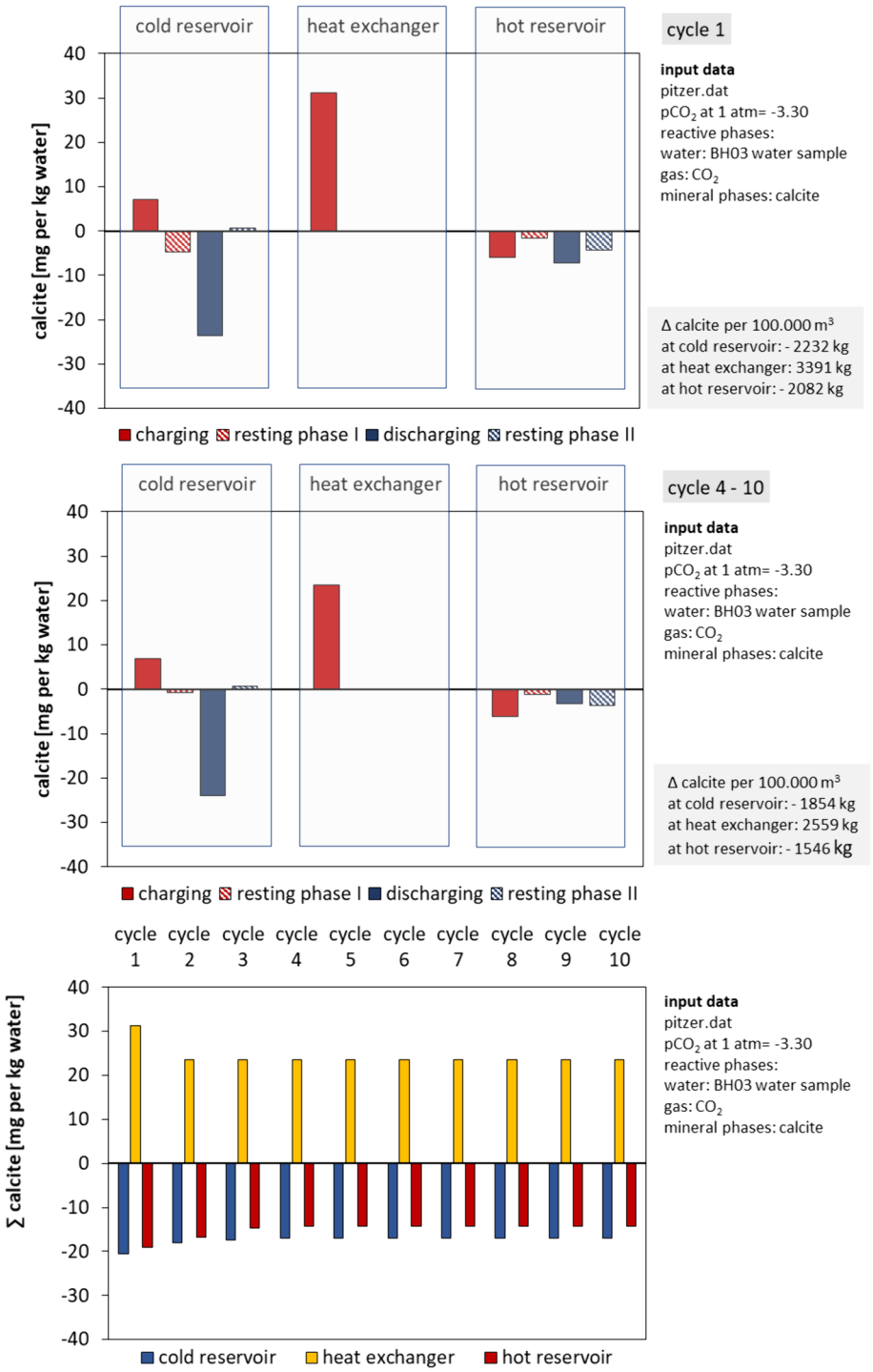

Fig. 13 Simulation results for the calcite precipitation and dissolution at three spots of an HT-ATES system during several cycles of charging, resting, and discharging phases of the hot reservoir for cycle 1 (top), cycles 4–10 (middle), and the total sum of calcite dissolution and precipitation of each cycle (bottom)

this amounts to 3391 kg. In the hot reservoir, the water cools down during the resting phase and its saturation decreases. To restore equilibrium, calcite dissolves and becomes enriched in the fluid. Since the hot reservoir experiences a certain temperature drop in

each of the four phases, calcite dissolves with each cycle. After the fluid is discharged and cooled down back to aquifer temperature, and then injected into the cold reservoir, more calcite dissolves to return to equilibrium with the surrounding aquifer.

These cycles of dissolution and precipitation are strongly connected to aquifer material and temperature, decreasing in the early years of operation and stabilizing at a constant rate after 4 years as temperature equilibria are reached in both the cold and hot reservoir. As mentioned above, pCO_2 is a sensitive parameter in the context of the calcium-carbonate equilibrium. In the calculations presented here, pCO_2 has been taken from downhole samples and adjusted for depth and pressure, assuming a minimum operating pressure of 5 bar at the surface. If this pressure can be increased, more CO_2 will remain dissolved in the water, resulting in less calcite precipitation due to the temperature increase. The same effect can be achieved by adding CO_2 to the water. This approach of CO_2 conditioning of the fluid to prevent calcite precipitation has been tested in various HT-ATES projects, such as aquifer heat storage tests in carbonates of the Bavarian Molasse Basin (Ueckert and Baumann, 2019), and at the siliciclastic HT-ATES demonstration site in Middenmeer, the Netherlands (Oerlemans et al. 2022). However, the addition of CO_2, particularly in carbonate systems, was found to harden the water and promote calcite dissolution.

These PhreeqC calculations examine only calcite saturation without considering other processes that also affect the precipitation reaction and kinetics such as the complexation of calcium and magnesium with organic acids or the formation of CO_2 due to the mineralization of organic matter and microbial activity. Moreover, the interaction of the fluid with a naturally occurring heterogeneous aquifer and, thus, with mineral phases such as dolomite and siderite was neglected and the reaction kinetics of barite, amorphous silica and, importantly, anhydrite/gypsum were not included in the model. Despite these limitations, the model demonstrates how sensitive the calcite saturation index reacts to HT-ATES operation and that, particularly with the recurrent equilibrium process, significant amounts of calcite can precipitate in the heat exchanger with each cycle. Conversely, calcite dissolution can be expected in both reservoirs.

Conclusion

In this study, the formation fluids of three wells targeting the Middle Triassic Schaumkalk in Berlin (Germany) at a former gas storage site on top of a salt structure were investigated to determine their origin and the potential use of this geological formation as HT-ATES.

Despite the long-term injection of water from the Bunter (Detfurth) formation into the Schaumkalk formation, the results of water analysis and numeric modeling indicate that the water from these wells is predominantly from the Muschelkalk formation and has been subject to evaporation processes and various rock–water interactions. This is the first time that Schaumkalk formation water was comprehensively characterized in the North German Basin. The observation of the fast disappearance of the Bunter water from the vicinity of the Muschelkalk wells can be explained by transport along faults and fractures to deeper parts of the reservoir.

In areas affected by salt tectonics, these geological aquifer conditions may be transferable to other locations in the North German Basin. For a HT-ATES system, this

implies the risk that the injected heated water would not remain in place. On the other hand, the permeability is high and high flowrates could be applied for producing and injecting the water, which is very beneficial for an HT-ATES operation. However, further investigations with larger volumes of injected water—ideally heated and with added tracers—are required to assess this.

The simulation of geochemical processes during a long-term HT-ATES application showed that calcite dissolution occurs both in the hot and cold reservoir and calcite precipitation on the heat exchanger. This precipitation is quite significant as up to 3391 kg calcite could form in 3 months of operation (38 kg/d). This could induce a problem for operators. However, the calculations do not consider kinetic restrictions of precipitation. Thus, this simulation alone cannot tell if and where the precipitation will actually occur. Measures to prevent scaling in the first place are the application of calcite inhibitors or the injection of CO_2 to control the pH and, thus, prevent calcite scaling.

The analysis of the chemical composition of the fluid water and gases further revealed several geochemical processes and microbial activity possibly resulting in corrosion occurring in the wells. Those reactions are typical for old wells targeting not only geothermal reservoirs but also former oil and gas formations. The reopening of those wells and reusing them for ATES or geothermal heat extraction is becoming a very interesting aspect of reusing the idle wells for sustainable energy production. The results from the simulation of HT-ATES at this site are generally transferable to other ATES systems that are planned to be installed in carbonate aquifers.

Abbreviations

HT-ATES	High-temperature aquifer thermal energy storage
MD:	Measured depth
NGB	North German Basin
URG	Upper Rhine Graben
MB	Molasse Basin
EC	Electrical conductivity
DO	Dissolved oxygen
ORP	Oxidation–reduction potential
IC	Ion chromatography
ICP-OES	Inductively coupled plasma-optical emission spectrometry
DOC	Dissolved organic carbon
TOC	Total organic carbon
XRD	X-ray powder diffractometer
GMWL	Global meteoric water line

Acknowledgements

We would like to thank the Federal Ministry for Economic Affairs and Climate Action (BMWK) for funding the ATESiQ project. We thank the laboratories of Hydroisotop GmbH, TU Berlin, TUB Freiberg, University of Bern and the GFZ. In addition, we thank Christian Cunow, Florian Lüdicke, and Stefan Kranz for their support during the field work. We would also thank Berliner Erdgasspeicher (BES GmbH) for their support.

Author contributions

LV: planned and conducted the field monitoring, data interpretation, developed and analyzed the models, writing. SR: field work, data interpretation, discussion. GB: project coordinator, planned the field work. CW: core sampling, discussion. AA and JK: microbiological monitoring, discussion. TW and MZ: gas monitoring. AS: XRD analysis. CT: fieldwork, discussion.

Funding

Open Access funding enabled and organized by Projekt DEAL. Open Access funding enabled by the project "Piloting Underground Storage of Heat In geoThermal reservoirs-PUSH-IT [EU: 1011096566]". This research was conducted as part of the projects "Geothermische Nutzung der Karbonatgesteine im norddeutschen Becken-ATES iQ: [BMWK: FKZ 03EE4013]" and "Geothermische Fernwärmeversorgung in Berlin–GeoFern [BMWK: FKZ 03EE4007]".

Availability of data and materials
The datasets generated, used, and/or analyzed during the current study are partly included in this published article, and all are available from the corresponding author on reasonable request.

Declarations

Competing interests
The authors declare that they have no competing interests.

Received: 28 March 2024 Accepted: 4 August 2024
Published online: 28 August 2024

References

Beernink S, Hartog N, Vardon PJ, Bloemendal M. Heat losses in ATES systems: the impact of processes, storage geometry and temperature. Geothermics. 2024. https://doi.org/10.1016/j.geothermics.2023.102889.
Bernard BB, Brooks JM, Sackett WM. Natural gas seepage in the Gulf of Mexico. Earth Planet Sci Lett. 1976;31(1):48–54. https://doi.org/10.1016/0012-821X(76)90095-9.
Bernasconi SM, Meier I, Wohlwend S, Brack P, Hochuli PA, Bläsi H, Wortmann UG, Ramseyer K. An evaporite-based high-resolution sulfur isotope record of late permian and triassic seawater sulfate. Geochimica et Cosmochimica Acta. 2017;204:331–49. https://doi.org/10.1016/j.gca.2017.01.047.
BGR, LAGB, LBEG, LBGR, LLUR,LUNG. (2022). Geologisches 3D-Modell Tieferer Untergrund Norddeutsches Becken (TUNB) https://gst.bgr.de
Blöcher G, Regenspurg S, Kranz S, Lipus M, Pei L, Norden B, Reinsch T, Henninges J, Siemon R, Orenczuk D, Zeilfelder S, Scheytt T, Saadat A. Best practices for characterization of high temperature-aquifer thermal energy storage (HT-ATES) potential using well tests in Berlin (Germany) as an example. Geothermics. 2024. https://doi.org/10.1016/j.geothermics.2023.102830.
Blöcher, G., Deon, F., Wenzlaff, C., Winterleitner, G., Regenspurg, S.,Virchow, L. (2023). *Abschlussbericht des Vorhabens Geothermische Nutzung der Karbonat-gesteine im Norddeutschen Becken ATES iQ*.
Brons HJ, Griffioen J, Appelo CAJ, Zehnder AJB. (Bio)geochemical reactions in aquifer material from a thermal energy storage site. Water Res. 1991;25(6):729–36. https://doi.org/10.1016/0043-1354(91)90048-U.
Burke WH, Denison RE, Hetherington EA, Koepnick RB, Nelson HF, Otto JB. Variation of seawater 87Sr/86Sr throughout phanerozoic time. Geology. 1982;10(10):516–9.
Chen C, Zhong H, Wang X, Ning M, Wang X, Ge Y, Wang H, Tang R, Hou M. Thermodynamic and kinetic studies of dolomite formation: a review. Minerals. 2023. https://doi.org/10.3390/min13121479.
Cherubini Y, Cacace M, Scheck-Wenderoth M, Noack V. Influence of major fault zones on 3-D coupled fluid and heat transport for the Brandenburg region (NE German Basin). Geothermal Energy Sci. 2014;2(1):1–20. https://doi.org/10.5194/gtes-2-1-2014.
Collignon M, Klemetsdal OS, Moyner O, Alcanie M, Rinaldi AP, Nilsen H, Lupi M. Evaluating thermal losses and storage capacity in high-temperature aquifer thermal energy storage (HT-ATES) systems with well operating limits: insights from a study-case in the Greater Geneva Basin Switzerland. Geotherm. 2020. https://doi.org/10.1016/j.geothermics.2019.101773.
Craig H. Isotopic variations in meteoric waters. Science. 1961;133:1702–3. https://doi.org/10.1126/science.133.3465.1702.
Daniilidis A, Mindel JE, Filho FD, Guglielmetti L. Techno-economic assessment and operational CO2 emissions of high-temperature aquifer thermal energy storage (HT-ATES) using demand-driven and subsurface-constrained dimensioning. Energy. 2022. https://doi.org/10.1016/j.energy.2022.123682.
Feldbusch E, Wiersberg T, Zimmer M, Regenspurg S. Origin of gases from the geothermal reservoir Groß Schönebeck (North German Basin). Geothermics. 2018;71:357–68. https://doi.org/10.1016/j.geothermics.2017.09.007.
Fleuchaus P, Godschalk B, Stober I, Blum P. Worldwide application of aquifer thermal energy storage—a review. Renew Sustain Energy Rev. 2018;94:861–76. https://doi.org/10.1016/j.rser.2018.06.057.
Fleuchaus P, Schuppler S, Stemmle R, Menberg K, Blum P. Aquifer thermal energy storage (ATES) in Germany. Grundwasser. 2021;26(2):123–34. https://doi.org/10.1007/s00767-021-00478-y.
Fontes JC, Matray JM. Geochemistry and origin of formation brines from the Paris Basin, France Brines associated with Triassic salts. Chem Geol. 1993;109(1):149–75.
Franz, M., Röhling, H.-G., Röhling, S.,Luppold, F. Der Muschelkalk des Norddeutschen Beckens. Deutsche Stratigraphische Kommission. Stratigraphie von Deutschland XIII Muschelkalk. Berlin: Koordination und Redaktion: Hagdorn, H., Simon, T., für die Subkommission Perm-Trias. Stratigraphie von Deutschland XIII Muschelkalk. - Schriftenr. Dt. Ges. Geowiss., 91; 2020. p. 621–662.
Frick M, Kranz S, Norden B, Bruhn D, Fuchs S. Geothermal resources and ATES Potential of Mesozoic reservoirs in the North German Basin. Energies. 2022. https://doi.org/10.3390/en15061980.
Göthel, M. 2016. Lithologische Interpretation und stratigraphisches Niveau der reflexionssesmischen Horizonte im Untergrund Brandenburgs einschliesslich Berlins. Brandenburg.geowiss Beitr. https://doi.org/10.1016/0883-2927(93)90032-C
Griffioen J, Appelo CAJ. Nature and extent of carbonate precipitation during aquifer thermal energy storage. Appl Geochem. 1993;8:161–76.
Hagdorn, H., Menning, M., Nitsch, E., Simon, T. The Muschelkalk. 2022. Zeitschrift der Deutschen Gesellschaft für Geowissenschaften. https://doi.org/10.1127/zdgg/2019/0197

Hagdorn, H., Simon, T., Dittrich, D., Geyer, G., Kramm, E.,Voigt, T. 2021. Lithostratigraphie der Unterer-Muschelkalk-Subgruppe. Hagdorn, H. & Simon , T. (eds). Stratigraphie von Deutschland XIII. Muschelkalk. Schriftenreihe der Deutschen Gesellschaft für Geowissenschaften 91 451–494.
Hirschl, B., Schwarz, U., Weiß, J., Hirschberg, R.,Torliene, L. Berlin Paris-konform machen. Eine Aktualisierung der Machbarkeitsstudie„Klimaneutrales Berlin 2050" mit Blick auf die Anforderungen aus dem UN-Abkommen von Paris. im Auftrag des Landes Berlin, vertreten durch die Senatsverwaltung für Umwelt, Verkehr und Klimaschutz. 2021
Holm TR, Eisenreich SJ, Rosenberg HL, Holm NP. Groundwater geochemistry of shortterm ATES test cycles. Water Resourc Res. 1987;23:1005–19. https://doi.org/10.1029/WR023i006p01005.
Holmslykke HD, Kjøller C. Reactive transport modelling of potential near-well mineralogical changes during seasonal heat storage (HT-ATES) in Danish geothermal reservoirs. J Energy Storage. 2023;72:108653. https://doi.org/10.1016/j.est.2023.108653.
Holmslykke HD, Weibel R, Olsen D, Anthonsen KL. geochemical reactions upon injection of heated formation water in a danish geothermal reservoir. ACS Earth Space Chem. 2023;7(9):1635–47. https://doi.org/10.1021/acsearthspacechem.2c00285.
Hörbrand T, Baumann T, Moog HC. Validation of hydrogeochemical databases for problems in deep geothermal energy. Geother Energ. 2018. https://doi.org/10.1186/s40517-018-0106-3.
Horita J, Zimmermann H, Holland HD. Chemical evolution of seawater during the Phanerozoic: Implications from the record of marine evaporites. Geochimica et Cosmochimica Acta. 2002;66(21):3733–56. https://doi.org/10.1016/S0016-7037(01)00884-5.
Jenne, E. A. Aquifer Thermal Energy (Heat and Chill) Storage. Intersociety Energy Conversion Engineering Conference; San Diego, California. 1992.
Jubitz K-B. Zur Regionalstellung der Rüdersdorfer Schaumkalkfazies im ostelbischen Unteren Muschelkalk Brandenburgs. Brandenburger Geowissenschaftliche Beiträg. 1994;1994(1):121–6.
Kampschulte A, Strauss H. The sulfur isotopic evolution of Phanerozoic seawater based on the analysis of structurally substituted sulfate in carbonates. Chem Geol. 2004;204(3–4):255–86. https://doi.org/10.1016/j.chemgeo.2003.11.013.
Korte C, Kozur HW, Bruckschen P, Veizer J. Strontium isotope evolution of late permian and triassic seawater. Geochimica et Cosmochimica Acta. 2003;67(1):47–62. https://doi.org/10.1016/S0016-7037(02)01035-9.
Kramm, E.,Hagdorn, H. Der Muschelkalk im östlichen Brandenburg und in der Lausitz. In: D. G. f. Geowissenschaften, editor. Stratigraphie von Deutschland XIII. Muschelkalk: Hagdorn, H., Simon, T.; 2021. p. 727–743.
Langmuir D. The geochemistry of some carbonate ground waters in central Pennsylvania. Geochimica et Cosmochimica Acta. 1971;35(10):1023–45. https://doi.org/10.1016/0016-7037(71)90019-6.
Leins A, Bregnard D, Vieth-Hillebrand A, Junier P, Regenspurg S. Dissolved organic compounds in geothermal fluids used for energy production: a review. Geother Energy. 2022. https://doi.org/10.1186/s40517-022-00220-8.
Linstow OV. Tektonik und Solführung im Untergrund von Berlin und Umgebend. Zeitschrift der Deutschen Geologischen Gesellschaft. 1922;74:89–100.
Mackenzie, F. T., Byrne, R. H.,Duxbury, A. C. (2024). *"Seawater"*. Encyclopedia Britannica, 22 Mar. 2024. Retrieved 27 Mar. https://www.britannica.com/science/seawater
McArthur JM, Howarth RJ, Bailey TR. Strontium isotope stratigraphy: LOWESS Version 3: best fit to the marine Sr-Isotope Curve for 0–509 Ma and accompanying look-up table for deriving numerical age. J Geol. 2001;109(2):155–70. https://doi.org/10.1086/319243.
Möller P, Weise SM, Tesmer M, Dulski P, Pekdeger A, Bayer U, Magri F. Salinization of groundwater in the North German Basin: results from conjoint investigation of major, trace element and multi-isotope distribution. Int J Earth Sci. 2007;97(5):1057–73. https://doi.org/10.1007/s00531-007-0211-1.
NLfB. Gutachten von Spülungsfiltrat und der beim Betrieb des Gasspeichers Berlin anfallenden Wässer in den Rüdersdorfer Schaumkalk des Muschelkalks. 1989
Noack V, Schroeder JH. Porosity development and distribution in the Rüdersdorfer Schaumkalk (Middle Triassic) of the Gas Store Berlin Germany. Facies. 2003;48(1):255–68. https://doi.org/10.1007/bf02667543.
Oerlemans, P., Drijver, B., Koenen, M., Koornneef, J., Dinkelman, D., Bos, W.,Godschalk, B. First field results on the technical risks and effectiveness of mitigation measures for the full scale HT-ATES demonstration project in Middenmeer. European Geothermal Congress 2022; Berlin2022.
Parkhurst DL, Appelo CAJ. Description of input and examples for PHREEQC version 3—a computer program for speciation, batch-reaction, one-dimensional transport, and inverse geochemical calculations US. GeoLogical Surv Techniques Methods. 2013. https://doi.org/10.3133/tm6A43.
Regenspurg S, Wiersberg T, Brandt W, Huenges E, Saadat A, Schmidt K, Zimmermann G. Geochemical properties of saline geothermal fluids from the in-situ geothermal laboratory Groß Schönebeck (Germany). Geochemistry. 2010;70:3–12. https://doi.org/10.1016/j.chemer.2010.05.002.
Regenspurg S, Blöcher G, Kranz S, Saadat A, Kharaka Y, Harmon R, Millot R, Shouakar-Stash O. Aluminium release by water-rock interaction during hydraulic tests in a siliciclastic aquifer in Berlin (Germany). Web Conf. 2019. https://doi.org/10.1051/e3sconf/20199807026.
Regenspurg S, Blöcher G, Bregnard D, Hehn V, Huenges E, Junier P, Kieling K, Kluge C, Kranz S, Leins A, Vieth-Hillebrand A, Wiersberg T, Zimmer M. Geochemical and microbial processes in a deep geothermal well during seven years of production stop and their potential impact on the well performance. Geothermics. 2024;120:102979. https://doi.org/10.1016/j.geothermics.2024.102979.
Stober I. Hydrochemical properties of deep carbonate aquifers in the SW German Molasse basin. Geothermal Energy. 2014;2(1):13. https://doi.org/10.1186/s40517-014-0013-1.
Stober I, Jodocy M, Burisch M, Person R. Tiefenwässer im Oberen Muschelkalk-Aquifer des Oberrheingrabens und des Südwestdeutschen Molassebeckens. Grundwasser. 2013;18(2):117–27. https://doi.org/10.1007/s00767-013-0224-6.
Stober, I., Birner, J.,Wolfgramm, M. Hydrochemie der Tiefenwässer in Deutschland. Zeitschrift für geologische Wissenschaften. 2014. 41 339–380

Stober I, Grimmer J, Kraml M. The Muschelkalk aquifer of the Molasse basin in SW-Germany: implications on the origin and development of highly saline lithium-rich brines in calcareous hydrothermal reservoirs. Geothermal Energy. 2023. https://doi.org/10.1186/s40517-023-00270-6.

Stricker K, Egert R, Schill E, Kohl T. Risk of surface movements and reservoir deformation for high-temperature aquifer thermal energy storage (HT-ATES). Geother Energy. 2024. https://doi.org/10.1186/s40517-024-00283-9.

Tarkowski R, Czapowski G. Salt domes in Poland—potential sites for hydrogen storage in caverns. Int J Hydrogen Energy. 2018;43(46):21414–27. https://doi.org/10.1016/j.ijhydene.2018.09.212.

Thiem, S., Müller, U., Budach, I., Wunsch, M., Flores Estrella, H., Himmelsbach, C., Hebold, J.,Hemmatabady, H. (2023). *Potenzialstudie Mitteltiefe Geothermie Berlin, Aufbau eines 3D-Untergrundmodells und Parametrisierung potenzieller Nutzhorizonte*.

Ueckert M, Baumann T. Hydrochemical aspects of high-temperature aquifer storage in carbonaceous aquifers: evaluation of a field study. Geother Energy. 2019. https://doi.org/10.1186/s40517-019-0120-0.

Wenzlaff, C., Winterleitner, G., Virchow, L., Regenspurg, S., Thielke, C.,Blöcher, G. (2022). *Assessing the geological potential of the Lower Muschelkalk as High Temperature - Aquifer Thermal Energy Storage (HT-ATES) horizon in Berlin (Germany)*. https://doi.org/10.5194/egusphere-egu22-7500

Wiersberg, T., Seibt, A.,Zimmer, M. Gas-Geochemische Untersuchungen an Formationsfluiden des Rotliegend der Bohrung Groß Schönebeck 3/90. Scientific Technical Report; 04/03. Sandsteine im In-situ-Geothermielabor Groß Schönebeck: Reservoircharakterisierung, Stimulation, Hydraulik und Nutzungskonzepte. Huenges, Ernst and Wolfgramm, Markus ed: GeoForschungsZentrum. 2004. p. 153–170.

Zhang B, Krause M, Mutti M. The Formation and structure evolution of Zechstein (Upper Permian) Salt in Northeast German Basin: a review. Open J Geol. 2013. https://doi.org/10.4236/ojg.2013.38047.

Zwenger W, Koszinski A. Die lithostratigraphische Gliederung des Unteren Muschelkalks von Rüdersdorf bei Berlin (Mittlere Trias, Anisian). Brandenburg Geowiss Beiträge. 2009;16:29–53.

Publisher's Note

Springer Nature remains neutral with regard to jurisdictional claims in published maps and institutional affiliations.